The mechanism of DNA replication termination in vertebrates

Citation	Dewar, James M., Magda Budzowska, and Johannes C. Walter. 2015. "The mechanism of DNA replication termination in vertebrates." Nature 525 (7569): 345-350. doi:10.1038/nature14887. http://dx.doi.org/10.1038/nature14887.
Published Version	doi:10.1038/nature14887
Citable link	http://nrs.harvard.edu/urn-3:HUL.InstRepos:26318589
Terms of Use	This article was downloaded from Harvard University's DASH repository, and is made available under the terms and conditions applicable to Other Posted Material, as set forth at http://nrs.harvard.edu/urn-3:HUL.InstRepos:dash.current.terms-of-use#LAA

The mechanism of DNA replication termination in vertebrates

James M. Dewar[1], **Magda Budzowska**[1], and **Johannes C. Walter**[1,2]

[1]Department of Biological Chemistry and Molecular Pharmacology, Harvard Medical School, Boston, MA 02115, USA

[2]Howard Hughes Medical Institute

Abstract

Eukaryotic DNA replication terminates when replisomes from adjacent replication origins converge. Termination involves local completion of DNA synthesis, decatenation of daughter molecules, and replisome disassembly. Termination has been difficult to study because termination events are generally asynchronous and sequence non-specific. To overcome these challenges, we paused converging replisomes with a site-specific barrier in *Xenopus* egg extracts. Upon removal of the barrier, forks underwent synchronous and site-specific termination, allowing mechanistic dissection of this process. We show that DNA synthesis does not slow detectably as forks approach each other and that leading strands pass each other unhindered before undergoing ligation to downstream lagging strands. Dissociation of CMG helicases occurs only after the final ligation step, and is not required for completion of DNA synthesis, strongly suggesting that converging CMGs pass one another and dissociate from double-stranded DNA. This termination mechanism allows rapid completion of DNA synthesis while avoiding premature replisome disassembly

DNA replication occurs in three broad stages: initiation, elongation, and termination. Termination occurs when converging replication forks meet and involves at least four processes, not necessarily in the following order. First, the last stretch of parental DNA between forks is unwound ("dissolution") and replisomes come into contact; second, any remaining gaps in the daughter strands are filled in and nascent strands are ligated ("ligation"); third, double-stranded DNA intertwinings (i.e. catenanes) are removed ("decatenation"); fourth, the replisome is disassembled. Despite decades of research on termination[1], we know little about the order, mechanism, and regulation of the above events, especially during eukaryotic chromosomal replication.

Termination has been most extensively studied in the mammalian DNA tumor virus SV40[2], where converging replication forks stall during termination[1,3,4]. Dissolution during SV40 replication requires rotation of the entire fork to produce catenations behind the fork (pre-catenanes)[5,6], which are resolved by Topo II[6], probably in a manner similar to how Topo IV functions during bacterial termination[7,8]. The SV40 replicative helicase, large T antigen (T-ag), dissociates from chromatin prior to dissolution, but whether this is required for the completion of replication is unknown[9,10]. After dissolution, daughter strands retain gaps of $\sim$60 nucleotides[11], which are ultimately filled in by an unknown mechanism in parallel to decatenation[12].

Eukaryotic termination has also been investigated. Although convergent forks accumulate at certain replication pause sites in yeast cells lacking 5'-3' DNA helicases[13–15], it is unknown whether forks stall during unperturbed termination. Furthermore, Topo II is not required for dissolution in budding yeast[16,17] or during vertebrate termination[18,19]. Recent work shows that late in S phase, the eukaryotic replicative helicase CMG (CDC45, MCM2–7, GINS)[20–23] is removed from chromatin by the ATPase p97 following ubiquitylation of MCM7 (by SCF[Dia2] in yeast)[24,25]. While one study implies that DNA replication can go to completion in the absence of CMG unloading[24], another reports that tracts of unreplicated DNA remain in the absence of this process[25]. Given that mis-regulation of bacterial termination can readily trigger re-replication of DNA[26,27], a potent driver of genomic instability in mammalian cells[28], a better understanding of eukaryotic termination is essential.

Owing to stochastic origin firing[29,30] and variable rates of replisome progression[31,32], the location and timing of eukaryotic termination is variable[30,33], making this process difficult to study. Here, we report that *Xenopus* egg extracts can be used to induce synchronous and localized termination events. This approach has allowed us to identify and order key events underlying vertebrate termination.

A system to study replication termination

Our strategy was to stall forks on either side of a reversible replication fork barrier (Fig. 1A-i-iii), and subsequently disassemble the barrier to trigger localized and synchronous termination events (Fig. 1A–iv). The barrier we employed consisted of an array of *lac* repressors (LacRs) bound to *lac* operators (*lacOs*)[34,35], which can be disrupted by IPTG. We constructed p[*lacO*x16], which contains 16 tandem copies of *lacO* (490 basepairs). p[*lacO*x16] was incubated in nucleus-free *Xenopus* egg extract, which promotes sequence-non-specific replication initiation on added DNA molecules, followed by a single, complete round of DNA synthesis via a mechanism that appears to reflect events in cells[36]. To monitor replication, radioactive [α-^{32}P]dATP was included in the reaction. When p[*lacO*x16] was replicated in the absence of LacR for $\sim$5 minutes and then cut with XmnI (Fig. 1Aiii), a single linear species representing fully replicated daughter molecules was observed (Fig. 1C, lane 1). In contrast, in the presence of LacR, a slow-mobility product appeared (Fig. 1C, lane 4) that corresponds to a double-Y structure, as shown by 2-D gel electrophoresis (Extended Data Fig. 1A). To confirm that the double-Y resulted from fork stalling at the outer edges of the array, we separately monitored replication in the plasmid

backbone and in the *lacO* array. In the presence of LacR, synthesis of the array was specifically delayed (Extended Data Figure 1F). In contrast, LacR had no effect on replication of a plasmid lacking *lacO* sites (Extended Data Fig. 1E). These results indicate that replication forks stalled on both sides of the LacR array, consistent with previous findings[34,35,37].

We next addressed whether replication forks stalled by LacR could restart. When IPTG was added to double-Y structures 5 minutes after replication initiation, 90% were converted to unit-sized linear plasmid molecules within a further 1.5 minutes (Fig, 1C, lanes 5–10 and Fig. 1H, yellow circles). In the absence of IPTG, only 21% of double-Y molecules disappeared after 3 minutes (Fig. 1C, lane 18). The conversion of double-Ys to linear species occurs when any remaining parental DNA holding daughter molecules together is unwound (Fig. 1B). This process, which we refer to as "dissolution," represents a convenient means to measure when converging replisomes meet. Notably, the ATR-Chk1 pathway was not activated above background levels during this procedure (Data not shown).

After dissolution, nascent strands should undergo ligation. To detect the growth and ligation of nascent strands, we digested p[*lacO*x16] with AlwNI, which cuts the plasmid once, ~550 nts from the rightward edge of the array and ~2000 nts from its leftward edge (Fig. 1Aiii and 1D), and we analyzed the products on a denaturing gel. Before IPTG addition, discrete species of ~2000 nts (Fig. 1E, Lane 4) and ~550 nts (Extended Data Fig 2A, lane 4) were observed. Upon IPTG addition, both bands grew heterogeneously (Fig. 1E and Extended Data Fig 2A). Since all leading strands were immediately extended upon IPTG addition (Extended Data Fig 2B–C), we infer that the heterogeneity observed resulted because growth of the lagging strand was delayed until ligation of an additional Okazaki fragment. Finally, the nascent strands increased abruptly to the full length of 3100 nts as ligation to downstream lagging strands occurred (Fig. 1E, Lanes 9–13). As expected, dissolution preceded ligation, and there was a ~45s delay between these two events (Fig. 1H).

Another important event associated with termination is decatenation of daughter molecules[18]. To measure this process, we analyzed undigested replication products on native agarose gels (Fig. 1F–G). Before addition of IPTG, when the array had not yet been duplicated, replication products migrated as a compact smear of high molecular weight, θ structures (Fig. 1F and Fig. 1G, lane 4). Upon addition of IPTG, most θs were lost within one minute, and they were successively converted into three types of dimeric catenanes described previously[5,18,38]: nicked-nicked (n–n), nicked-supercoiled (n-sc), and supercoiled-supercoiled (sc-sc) (Fig. 1G and Extended Data Fig. 3A). n-n catenanes appeared first (Fig. 1G, Lanes 7–8), followed by n-sc (lanes 8–10), and sc-sc (Fig. 1G Lanes 9–12). Supercoiling is the result of nucleosome assembly on closed circular DNA[39]. Finally, monomeric, supercoiled daughter molecules accumulated (sc, Fig. 1G, Lane 17) dependent on Topoisomerase II (Extended Data Fig 3B–D) as seen *in vivo*[16,17]. Topo II was not required for dissolution or ligation (Extended Data Fig 3C–D) suggesting these processes proceed independently of decatenation[16,17,19]. Like ligation, decatenation began ~40s after dissolution, but progressed at a slower rate than ligation (Fig. 1H>). The same intermediates were detected in the absence of LacR, but their order of appearance was not well-defined (Extended Data Fig. 3E).

Our results demonstrate that a reversible replication fork barrier allows induction of a synchronous and spatially defined termination event. They also show that soon after forks meet, as measured by dissolution, daughter molecules are quickly ligated and decatenated.

Converging replication forks do not stall

To test the proposal that replication forks slow down or stall during termination[1,3,4], we quantified the rate of DNA synthesis as two replisomes converged within the *lacO* array. To minimize the loss of synchrony among replisomes after IPTG addition, we used a 365 bp array containing only 12 copies of *lacO*, which was sufficient to prevent dissolution at the 5 minute time point (Extended Data Fig. 4C). We replicated p[*lacO*x12] in the presence of LacR, added IPTG after 5 minutes, and examined subsequent replication within the array by cutting the plasmid with AflIII and PvuII (Fig. 2A). The rate of DNA synthesis within the array was almost perfectly linear after IPTG addition (Fig. 2B–C) even as dissolution was underway. These data suggest that converging forks do not slow significantly before they meet. A similar conclusion was reached when radiolabelled nucleotides were added at the same time as IPTG and incorporation measured only during the final stage of replication on p[*lacO*x12] (Extended Data Fig. 5A–F) or p[*lacO*x16] (Extended Data Fig 5G–H). Moreover, fork rates within the *lacO* array resembled those previously reported in the same egg extracts (Extended Data Fig. 5F). These results suggest that converging replisomes do not undergo prolonged stalling.

To further evaluate whether forks slow or stall upon encounter with a converging fork, we compared progression of leading strands into arrays containing 12 (12x*lacO*) or 32 copies (32x*lacO*) of *lacO* (Fig. 3A), in which the rightward fork should collide with a converging fork at the 6th or 16th *lacO* repeats, respectively (Fig. 3A). If converging forks interfere with each other, the rightward leading strand should pause or stall near the 6th repeat in p[*lacO*x12] but not in p[*lacO*x32]. As expected, dissolution (Figure 1B) happened much earlier on p[*lacO*x12] than on p[*lacO*x32] (Extended Data Fig. 6A–D). To monitor leading strand progression into the array with near-nucleotide resolution, DNA intermediates were purified, digested with the nicking enzyme Nt.BspQI, which released *rightward* leading strands (Fig 3A), and separated on a denaturing polyacrylamide gel (Fig 3B). Prior to IPTG addition, a discrete ladder of leading strands was seen (Fig 3B, Lanes 2,14), in which the 3' ends of leading strands stalled ∼29–33 nts from each LacR molecule in the array. This ∼30 nucleotide gap likely corresponds to the footprint of the CMG complex[35,40]. As shown in Fig. 3B (red lines) and quantified in Extended Data Fig. 6E, 78% of leading strands were stalled at the first 3 *lacO* sites, indicating that most replisomes were blocked at the outer edges of the array.

Upon addition of IPTG, extension of leading strands resumed immediately (Fig. 3B, lanes 3–11 and 15–23). Importantly, there was no enhanced pausing near the 6th *lacO* repeat of the 12x*lacO* array versus the 32x*lacO* array. By 5.67 minutes, the majority of leading strands had extended beyond the sixth *lacO* repeat within both arrays (Fig. 3B, lanes 6 and 18 and Extended Fig. 2C). This was also true for the *leftward* leading strands (Extended Data Fig. 6F–G). Furthermore, leading strands were extended beyond the 6th *lacO* repeat in the *lacO*x12 and *lacO*x32 arrays with similar kinetics (Fig. 3C–D). When leading strands were

analyzed on alkaline denaturing gels, we observed that all rightward and leftward leading strands passed the mid-point of the array by 6.25 min (Extended Data Fig 2D–E), indicating that the converging leading strands were readily extended past each other. In summary, we failed to observe detectable slowing or pausing of DNA synthesis during termination, and converging leading strands passed each other unhindered, implying that converging replisomes do not pause or stall significantly.

Lagging strand gaps are rapidly filled in

During SV40 replication termination, gaps of ~60 nucleotides persist following dissolution[11]. To determine if the appearance of such gaps precedes the ligation step in our system, we mapped the 3' ends of the *leftward* leading strands and the 5' ends of the *rightward* lagging strands during termination within *lacO*x12 (Fig. 4A). To this end, we digested DNA intermediates with Nb.BbvCI or Nb.BtsI to release leading or lagging strands, respectively (Fig. 4A>), and separated them on denaturing polyacrylamide gels. Following IPTG addition, we detected a prominent leading strand product beyond the twelfth *lacO* repeat (species 274 in Fig. 4B; the 3' and 5' termini of all leading and lagging strand products, respectively, are mapped relative to the Nb.BtsI site) as seen also in Figure 3B. The 3' end of this species was located ~3 nucleotides from the 5' end of the most abundant lagging strand product of the converging fork (271, Fig. 4C). We observed many other, less prominent leading stra), most of which mapped close to corresponding lagging strand products (176–417, Fig. 4C). The results show that leading strands are generally extended to within ~3 nucleotides of the lagging strands (Fig. 4D). It is likely that leading strands immediately abut lagging strands and that the ~3 nucleotide gap reflects imprecise mapping of lagging strands (see methods). In conclusion, we observe no evidence of persistent gaps between leading and lagging strands during replication termination.

CMGs dissociate late during termination

To determine when replisome components dissociate during termination, we monitored MCM7, CDC45, Polε and RPA binding to a site flanking the *lacO* array using Chromatin ImmunoPrecipitation (ChIP) (*FLK2* locus, Extended Data Fig 7A). In parallel, we monitored dissolution, ligation, and decatenation. Prior to IPTG addition, MCM7, CDC45, Polε, and RPA were 4–8-fold enriched at the array in the presence of LacR compared to buffer (Extended Data Fig. 7B–E, Fig. 5 min time point), demonstrating that the ChIP signal reflects replisome stalling at the array. When IPTG was added at 5 minutes, MCM7, CDC45, RPA and Polε largely dissociated by 9 minutes, whereas in the absence of IPTG, they dissociated much more slowly (Extended Data Fig. 7B–E). RPA dissociation correlated well with ligation, as expected, since ligation marks the disappearance of any ssDNA in the termination zone (Figure 5A, compare red squares and blue circles). Strikingly, CDC45, MCM7, and Pol ε dissociated ~1.5 minutes after dissolution and ~0.5 minutes after RPA dissociation and ligation (Figure 5A). A time course of ChIP at sequences adjacent to and within the array (Extended Data Fig. 7F–I) was consistent with MCM7, CDC45, and DNA Polε moving into the array and then back out following dissolution (Extended Data Fig. 7J). MCM7 and CDC45 also dissociated after dissolution during replication of plasmid DNA that lacked a *lacO* array (p[*empty*], Extended Data Fig. 8A–B). Although the delay between

ligation and unloading of MCM7 and CDC45 was not readily detectable on this template (Extended Data Fig. 8B) this was not surprising, given the asynchrony of termination in this setting. Together, the data support a model in which CDC45 and MCM7 dissociate late in termination, long after forks meet (dissolution) and shortly after ligation.

If our model is correct, inhibiting CMG unloading should not affect dissolution or ligation. To test this, we inhibited ubiquitin signaling, which is required for chromatin dissociation of CMG[24,25,41]. p[*empty*] was replicated in extracts that were incubated with vehicle or the de-ubiquitylating enzyme inhibitor ubiquitin-vinyl-sulfone (Ub-VS), which leads to the depletion of free ubiquitin[35,41], and we performed MCM7 and CDC45 ChIP. As shown in Fig. 5B–C, UbVS substantially delayed MCM7 and CDC45 dissociation, and this effect was partially reversed by co-addition of free ubiquitin (Fig 5B–C>). The same inhibitory effect of UbVS on CMG unloading was observed when plasmids were recovered from egg extract and blotted for MCM7 and CDC45 (Extended Data Fig. 8C). This analysis also confirmed prior reports[24,25] of MCM7 ubiquitylation during replication. Importantly, dissolution, ligation, and decatenation were not affected by Ub-VS (Fig 5D–E and Extended Data Fig 8F–I). We conclude that defective CMG unloading does not affect dissolution, ligation, or decatenation, strongly supporting our model that CMG unloading is a late event in replication termination.

Discussion

In this study, we present a novel approach to induce synchronous and site-specific replication termination. Using this system, we observe no slowing or pausing of DNA synthesis as forks converge (Fig. 5Ei-ii). Leading strands pass each other unhindered and immediately abut downstream lagging strands before undergoing ligation (Fig. 5E iii-v). CMG remains associated with DNA after dissolution, and it is unloaded only after the leading strand of one fork is ligated to the lagging strand of the opposing fork (Fig. 5E vii). Catenane removal is initiated at the same time as ligation (Fig. 5v–vi). In contrast to models of termination in which replication forks stall[1,3,4], our data imply that topological stress between replisomes is handled efficiently and that converging replisomes do not clash or that if they do, any remaining template DNA is immediately reeled into the stalled replisome for duplication (not shown). We previously showed that CMGs encircle the leading strand template at the replication fork[42]. Therefore, converging CMGs approach each other on opposite strands[42,43], which helps explain how they could pass each other. If a fork stalls (e.g. at the ribosomal DNA locus[13,14]) the same termination mechanism could still operate provided the stalled fork remains stable until a converging fork arrives. We expect this to be the case, given our recent observation that a single fork stalled at an ICL does not collapse or lose its CMG complex[34]. We speculate that at telomeres the replisome simply runs off the chromosome end. .

Our observations that CMG dissociates after the ligation step (Fig. 5A), and that ligation is not affected when CMG unloading is impaired (Fig 5B–C,E), strongly imply that CMG is unloaded from dsDNA. We propose that when CMG reaches the 5' end of the opposing fork's lagging strand, it passes over the ssDNA-dsDNA junction and keeps moving along dsDNA (Fig. 5E), as previously observed for purified MCM2–7 and CMG *in vitro* (see [23,44]

but see also [22]). This scenario is appealing, as it would prevent CMG from interfering with ligation of the nascent strands. We propose that CMG ubiquitylation and its removal by p97[24,25] is triggered once CMG encircles dsDNA. Such a mechanism would help to avoid inappropriate CMG unloading from active replication forks, where CMG encircles ssDNA. Our results disagree with a recent report, which concluded that inhibition of CMG unloading prevents completion of DNA synthesis[25]. In contrast, another report that defective CMG unloading does not prevent cell cycle progression[24] is consistent with our model. We recently reported that CMG can be unloaded from ssDNA when two replisomes collide with a DNA interstrand cross-link[41]. However, this process involves a unique, BRCA1-dependent pathway that is not employed during termination[41]. In conclusion, the termination mechanism described here allows rapid completion of DNA synthesis while minimizing the possibility of premature replisome disassembly.

Methods

Protein Purification

Biotinylated LacR was purified using a protocol adapted from Kenneth Marian's laboratory (Personal Communication). The LacR open reading frame was fused to a C-terminal AviTag (Avidity, Denver, CO) and expressed from pET11a (pET11a[LacR-Avi]). To biotinylate the AviTag on LacR-Avi, biotin ligase was co-expressed from pBirAcm (Avidity, Denver, CO). To this end, pET11a[LacR-Avi] and pBirAcm were co-transformed into T7 Express cells (New England Biolabs) and grown in the presence of ampicillin (100 μg/ml) and chloramphenicol (17 μg/ml). Expression of LacR-Avi and the biotin ligase was induced by addition of IPTG to a final concentration of 1 mM. Cultures were supplemented with 50 μM biotin (Research Organics, Cleveland, OH) to ensure efficient biotinylation of LacR-Avi.

Cell pellets were resuspended in lysis buffer (50 mM Tris-HCl, pH 7.5, 5 mM EDTA, 100 mM NaCl, 1 mM DTT, 10% sucrose (w/v), cOmplete protease inhibitor (Roche, Nutley, NJ). The cells were lysed at room temperature in the presence of 0.2 mg/ml lysozyme and 0.1 % Brij 58. The insoluble, chromatin-containing fraction was isolated by centrifugation at 4°C. Chromatin-bound LacR was then released by sonication (in 50 mM Tris-HCl, pH 7.5, 5 mM EDTA, 1 M NaCl, 1 mM DTT, cOmplete protease inhibitor, 30 mM IPTG). DNA was removed from the soluble fraction by addition of polymin P (final concentration 1%), LacR was precipitated by addition of ammonium sulphate (final concentration 37%). The precipitate was dissolved in wash buffer (50 mM Tris-HCl, pH 7.5, 1 mM EDTA, 2.5 M NaCl, 1 mM DTT, cOmplete protease inhibitor) and then applied to a column of SoftLink avidin resin (Promega, Madison, WI). LacR was eluted (in 50 mM Tris-HCl, pH 7.5, 1 mM EDTA, 100 mM NaCl, 1 mM DTT, 5 mM biotin) and dialyzed overnight (against 50 mM Tris-HCl, pH 7.5, 1 mM EDTA, 150 mM NaCl, 1 mM DTT, 38% glycerol (v/v)). Purified LacR was frozen in liquid nitrogen and stored at −80°C. A more detailed purification protocol is available upon request.

Cyclin A was purified as described previously[45]

Plasmid construction and preparation

pJD82 (Extended Data 9) was created by replacing the SacI-KpnI fragment of pBlueScript II KS- with the sequence:

GAGCTCTCACACCTACAAGGGATGTACATCAATTGTGAGCGGATAACAATT
GTTAGGGAGGAATTGTGAGCGGATAACAATTTGGAGTTGATAATTGTGAGC
GGATAACAATTGGCTTCAACGTAATTGTGAGCGGATAACAATTTCCGTACG
AATGTGCCGAACTTATGGTACC

This contains 4 tandem repeats of the *lac* operator sequence (AATTGTGAGCGGATAACAATT) interspersed by an average of 10–11 base pairs of random sequence (average 10.33 basepairs). Additional tandem repeats of the BsiWI-BsrGI fragment were then cloned into pJD82, and subsequently derived vectors, to generate arrays of 8, 12, 16, 32 and 48 *lacO* repeats (Extended Data 9). Recognition sites for nicking enzymes were introduced by QuickChange mutagenesis (Agilent Technologies, Santa Clara, CA) according to the manufacturer's guidelines.

To propagate *lacO* plasmid DNA, plasmids were transformed into DH5α cells and grown for a minimal number of passages in the presence of 2 mM IPTG. DNA was prepared using the QIAprep spin kit (Qiagen, Valencia, CA). To eliminate preparations containing genetic rearrangements (typically ∼25%) each preparation was separated by electrophoresis on a 0.8% agarose gel and visualized by ethidium bromide staining. Preparations that were free of rearranged plasmids were then verified by sequencing (Genewiz, Cambridge, MA).

Xenopus egg extracts and DNA replication

Xenopus egg extracts were prepared from *Xenopus laevis* wild type males and females 2–5 years of age, as approved by the Harvard Medical School Institutional Animal Care and use Committee (IACUC) and as described previously[46]. For DNA replication, 1 volume of 'licensing mix' was prepared by adding plasmid DNA to High Speed Supernatant (HSS) of egg cytoplasm to a final concentration of 7.5–15 ng/μl. Licensing mix was incubated for 30 minutes at room temperature, leading to the formation of pre-replication complexes (pre-RCs). Next, licensing mix was supplemented with 0.1 volumes of Cyclin A to a final volume of 576 nM and incubated a further 10 minutes at room temperature, as previously described[45]. Cyclin A treatment was performed to achieve highly synchronous DNA replication (Extended Data Fig. 10). Finally, 1.9 volumes of nucleoplasmic extract (NPE) was added to initiate Cdk2-dependent replication at pre-RCs. In all Figures, "0 minutes" represents the time 30 seconds after NPE addition. To radiolabel DNA, NPE was supplemented with [α-^{32}P]dATP. Reactions were stopped with 10 volumes Stop Solution (0.5% SDS, 25 mM EDTA, 50 mM Tris-HCl pH 7.5). DNA in Stop Solution was treated with RNase A (190 ng/μl final concentration) then Proteinase K (909 ng/μl final concentration) before either direct analysis by gel electrophoresis or purification of DNA as described previously[40]. For UbVS experiments, UbVS (Boston Biochem) was added to final concentration of 20 μM, to HSS 5 minutes prior to addition of plasmid DNA (HSS) and to NPE 5 minutes prior to addition of HSS, with or without 120 μM Ubiquitin (Boston Biochem). Unless otherwise stated in the figure legend, all experiments were performed at

least twice and a representative result is shown. Replicate samples were collected from independently assembled replication reactions, and therefore represent biological replicates.

Immunodepletions

To deplete Topo II-α from *Xenopus* egg extracts one volume of Protein A Sepharose Fast Flow (PAS) (GE Healthcare) was incubated with 4.5 volumes of affinity purified, anti-Topo II-α antibody raised against the C-terminal 20 residues (1 mg/ml). For mock depletion, an equivalent quantity of nonspecific IgGs were used. 5 volumes of pre-cleared HSS or NPE was then mixed with 1 volume of the antibody-bound sepharose and incubated for 45 min at 4°C, and for the NPE this was repeated once. Depleted extracts were collected and used immediately for DNA replication.

Induction of termination

To monitor termination, 0.05 volumes plasmid DNA (150–300 ng/μl) was incubated with 0.1 volumes LacR (54 μM) or dialysis buffer for at least 90 minutes at room temperature to allow formation of LacR arrays on the DNA. Licensing mix was prepared by adding 0.85 volumes of HSS, and DNA was replicated as described above. To induce termination, 0.06 volumes of IPTG was added (to a final concentration of 10 mM) at the time indicated (typically 5 minutes), which triggered dissociation of *lacO*-bound LacR. To accurately withdraw samples at the times indicated, reactions composed of the same Licensing Mix and NPE were staggered, where necessary.

2D gel electrophoresis

2D gels were performed as described[41]. Briefly, purified DNA was digested with XmnI (New England BioLabs) and then separated by native-native 2D gel electrophoresis. Samples were separated in the first dimension on a 0.4 % agarose gel at 0.75 V/cm for approximately 40 hours at room temperature. The gel was stained with 0.3 μg/ml ethidium bromide, allowing the 2–8 kilobase pairs size-range to be excised. A second dimension gel containing 1 % agarose and 0.3 μg/ml ethidium bromide was cast over the gel slice from the first dimension. DNA was separated on the second dimension at 4.5 V/cm for 12 hours at 4°C.

Termination assays

To monitor dissolution, 0.25–1.0 ng/μl of purified DNA was incubated in CutSmart Buffer with 0.4 units/μl of XmnI (New England BioLabs) at 37°C for 1 hour. Digested products were separated on a 1.2 % agarose gel at 4 V/cm and detected by autoradiography. Dissolution (%) was calculated as the percentage of total signal in each lane present in the linear products of digestion (Lins, Fig 1C).

To monitor ligation, 0.25–1.0 ng/μl of purified DNA was incubated in CutSmart buffer with 0.2 units/μl of AlwNI (New England BioLabs) at 37°C for 1 hour. Digests were terminated by addition of EDTA to 30 mM, then products were separated on a 1.5 % denaturing alkaline agarose gel at 1.5 V/cm and detected by autoradiography. The percentage of total signal in each lane present in the full-length strands (FLS) was measured (FLS, Fig 1E). During electrophoresis, partial hydrolysis caused signal from the FLS to smear down. To

correct for this, a fully ligated plasmid was cleaved and analyzed on the same gel. The percentage of signal in FLS band of the fully ligated plasmid was measured (FLS^{FL}) and used to correct signal in the other lanes to yield an accurate measure of ligation. Ligation (%) was calculated as $FLS/FLS^{FL}*100$

To monitor decatenation, 0.25–1.0 ng/μl of purified DNA was separated on a 0.8 % agarose gel at 4 V/cm and detected by autoradiography. Decatenation (%) was measured as the percentage of total signal in each lane present in circular monomers (CMs, Fig. 1G).

To monitor DNA synthesis within a *lacO* array (Figure 2), 0.25–1.0 ng/μl of purified DNA was incubated in Buffer 3.1 with 0.2 units/μl PvuII and 0.2 units/μl AflIII (New England BioLabs) at 37°C for 1 hour. Digested products were separated on a 1.2 % agarose gel at 4 V/cm and detected by autoradiography. To measure array synthesis (SYN^{ARY}), the 0.5–1.5 kb region of each lane was quantified (lins and DYs, Fig 2B). To measure vector synthesis (SYN^{VEC}), the 2 to 6 kb region of each lane was quantified, which included the ~3.0 and ~6.0 bands that arose when one, or both, lagging strands did not cut, respectively. Total signal in each lane (SYN^{TOT}) was also measured. To correct for differences in efficiency of DNA extraction, total lane signal was also measured in a set of unprocessed samples (SYN^{UN}), which were separated and detected in parallel. Array synthesis (%) was calculated as $SYN^{UN}/SYN^{TOT}*SYN^{ARY}$, vector synthesis was calculated as $SYN^{UN}/SYN^{TOT}*SYN^{VEC}$ and in both cases the 10 minute time point was assigned a value of 100%. The same approach was also used to quantify synthesis of the 294/794 bp fragments (quantified in the same manner as the array) and the 2354 bp fragments (quantified in the same manner as the vector fragments) in Extended Data Figure 1. In Figure 2 and Extended Data Figure 1, a longer exposure of the array fragment is shown because it is less intense than the vector fragment.

To analyze topoisomers (Extended Data Fig 3D) 0.25 ng/μl of radiolabelled DNA was incubated in 1X Buffer A and 1X Buffer B (Topogen) with 0.2 U/μl Human Topo II-α (Topogen) at 37°C for 15 minutes, or in CutSmart Buffer with 0.4 U/μl XmnI or 0.04 U/μl Nt.BspQI (New England Biolabs) for 1 hour.

Nascent strand analysis

To nick rightward leading strands, 1–2 ng/μl of purified DNA was incubated in Buffer 3.1 with 0.4 units/μl Nt.BspQI (New England BioLabs) at 37°C for 1 hour. To nick leftward leading strands, 1–2 ng/μl of purified DNA was incubated in CutSmart buffer with 0.04 units/μl Nb.BsrDI (New England BioLabs) at 65°C for 1 hour. To nick rightward leading strands closer to the *lacO* array, 1–2 ng/μl of purified DNA was incubated in CutSmart buffer with 0.04 units/μl Nb.BbvCI (New England BioLabs) at 37°C for 1 hour. To nick leftward lagging strands, 1–2 ng/μl of purified DNA was incubated in Buffer 3.1 with 0.04 units/μl Nb.BtsI (New England BioLabs) at 37°C for 1 hour. In all cases, nicking reactions were stopped by the addition of 0.5 volumes of Stop Solution B (95% formamide, 20 mM EDTA, 0.05% bromophenol blue, 0.05% xylene cyanol FF).

Nicked DNA (1.5–2 μl sample) was separated on a 42 cm long, 4 or 5 % polyacrylamide sequencing gel using Model S2 sequencing gel apparatus (Apogee Electrophoresis,

Baltimore, MD) according to the manufacturer's guidelines. To maximize the range of nascent products that could be resolved, gels were cast with a thickness gradient of 0.4 to 1.2 mm, beginning to end, to establish an electrical field gradient during electrophoresis. Sequencing gels were prepared with Rapidgel-XL in 0.8X GTG Buffer (USB Corporation, Cleveland). Sequencing ladders were generated using the Cycle Sequencing Kit (USB Corporation, Cleveland) with primers JDO107, JDO109, JDO110, JDO111 (Extended Data 9) and pJD150 (Extended Data 9) as template DNA.

Mapping and quantification of the Nascent strands in Fig. 3–Fig. 4 was performed as follows. Nascent leading and lagging strands were mapped using the sequencing ladders generated by the primers indicated in Fig. 3A and Fig. 4A (see Extended Data 9 for sequences). Slight discrepancies may exist between mapped and actual lagging strand product sizes (Fig. 4C) since the sequencing ladder (generated by JDO110 Fig. 4A) is complementary to the lagging strands. A fraction of lagging strand products 176–302 were not extended upon IPTG addition, probably because they were reached by the rightward leading strand first. Lagging strand products 312–417 appeared de novo after IPTG addition, and therefore represent growing lagging strands of the leftward fork. To quantify leading strand progression (Fig. 3C–D) leading strands whose 3' ends were located before *lacO7* (in Fig. 3B and data not shown) were quantified, and peak signal was assigned a value of 100 (%Max).

ChIP and quantitative PCR

ChIP and quantitative PCR (qPCR) were performed essentially as described[41]. Chromatin was withdrawn and crosslinked in the presence of 1% formaldehyde for 10 minutes at room temperature. Crosslinking was then quenched by the addition of 0.1 volumes glycine (1.25 M) for 10 minutes. Samples were then spun through Bio-Spin P-6 Gel (containing Tris Buffer, Bio-Rad) to remove salts and small molecules, before being stored in 10 volumes of sonication buffer (20 mM Tris pH 7.5, 150 mM NaCl, 2 mM EDTA, 1% IGEPAL CA-630 (v/v), 2 mM PMSF, 5 μg/μl aprotinin, 5 μg/μl leupeptin). Samples were then sonicated to shear chromatin into approximately 250 bp fragments.

The antibodies used were described previously[21,41]. Antibodies were incubated with chromatin overnight at 4°C, then immunoprecipitated by addition of Protein A-Sepharose Fast Flow beads (GE Healthcare) for 2 hours at room temperature. Beads were washed sequentially with sonication buffer, high salt buffer (sonication buffer supplemented with 500 mM NaCl and 100 mM KCl), wash buffer (10 mM Tris pH 7.5, 0.25 M LiCl, 1 mM EDTA, 0.5% NP-40 (v/v), 0.5% SDS (w/v)) and TE (10 mM Tris pH7.5, 1 mM EDTA), before being eluted into elution buffer (50 mM Tris pH7.5, 10 mM EDTA, 1% SDS) at 65°C for 20 minutes. Eluted chromatin, and input samples, were treated with RNase for 30 minutes at 37°C. Finally, proteins were degraded by addition of NaCl (250 mM final) and treatment with Pronase (2 μg/μl final) at 42°C for 6 hours. DNA-peptide crosslinks were reversed by treatment at 70°C for a further 9 hours. DNA was subsequently phenol:chloroform extracted and ethanol precipitated. The absolute amount of DNA recovered from the immunoprecipitated and input samples was measured by quantitative PCR (qPCR) relative to a standard curve. The qPCR primers used are listed in Extended

Data 9. Binding was measured as the percentage recovery of immunoprecipitated DNA, relative to the input (EXP^{REC}).

To minimize error in the ChIP process, an internal control was built into all experiments. *Xenopus* egg extracts were used to separately replicate a different plasmid, pQUANT (see Extended Data 9 for sequences). Mid-way through replication, pQUANT, was crosslinked, quenched, and spun through Bio-Spin P-6 gel (as above) to yield a single pool of heterologous chromatin that was bound by replication proteins. An equal amount of pQUANT chromatin was added to all experimental chromatin samples prior to sonication, and this was carried through the entire ChIP procedure. For each set of immunoprecipitations, the recovery of pQUANT (QNT^{REC}) should be identical between samples. To correct for technical variation in any set of immunoprecipitations, average pQUANT recovery was calculated (QNT^{AVG}) and normalized recovery (%) was calculated as EXP^{REC}*QNT^{AVG}/QNT^{REC}. This ensured that the only sources of technical variation were the crosslinking process and the qPCR. To maximize the reliability of the qPCR, these measurements were performed in quintuplicate and the median value was used. Where three ChIP experiments were combined and plotted as mean±s.d. (Fig 5A–C, Extended Data Figs 7F–I and 9L–M) it was necessary to normalize the data to correct for differences in absolute IP efficiency between experiments. For each protein measured by ChIP, mean recovery across all loci in all samples (mean^{all}) was calculated for each experiment (mean^{all1}, mean^{all2} and mean^{all3}) and used to generate a correction factor for each experiment (e.g. for experiment 1 the correction factor is [(mean^{all1}+mean^{all2}+mean^{all3})/3]/mean^{all1}). To measure dissociation (Fig 5A–C), recovery of the *FLK2* locus was measured (shown in Extended Data Fig 7F–I and Fig 8L–M) and peak signal was assigned a value of '0', while background signal (measured at 4 or 5 min for Fig 5A, or 10 min for Fig 5B–C) was assigned a value of 100. The experiments shown in Fig 5A and Extended Data Fig. 7F–I were repeated 3 times, once with p[*lacO*x12] and twice with p[*lacO*x16].

Plasmid pull downs

Plasmid pull downs were performed essentially as described[47], with the following exceptions. Beads were resuspended in buffer supplemented with 4% DMSO and 100 μM NMS-873[48] to block further CMG unloading once the samples were withdrawn[25]. Plasmid-associated proteins from 40–80 ng of plasmid were isolated, and a quarter of the sample was analyzed by Western blotting using previously-described antibodies against CDC45, MCM7, and PCNA[41].

HIS$_6$-Ub Immunoprecipitations

Ni-NTA Superflow Resin (Qaigen) was washed three times with Urea Buffer (10mM imidazole, 0.2% NP-40, 8 M urea, 500 mM NaH$_2$PO$_4$, 50 mM Tris HCl, pH 8.0). For each immunoprecipitation, 10 μl of resin was added per tube, and resuspended to 191 μl in Urea buffer. Extracts were supplemented with 100 μM of HIS$_6$-Ubiquitin (Boston Biochem) and replication was carried out as described above. At the indicated time, 9 μl of extract was mixed with the bead mix and samples were incubated for one hour at room temperature, with end-over-end rotation. Resin was washed three times with urea buffer. All residual buffer was removed, and resin was boiled for 5 minutes in 30 μl sample buffer (125 mM

Tris-HCl pH 6.8, 20% glycerol, 6.1% SDS, 0.01% bromophenol blue, 10% β-mercaptoethanol). 30 µl of 0.5 M imidazole was added to each sample and HIS$_6$-tagged proteins were eluted off the resin for 60' at room temperature, with gentle agitation. Resin was spun down at 1000 RCF for 1 minute, and the supernatant was removed. 10 µl of each sample was resolved on an SDS-PAGE gel alongside an input control and analyzed by Western blotting using the previously-described antibody against MCM7[49]. In extended Data Fig. 8D, a longer exposure of the IP lanes is shown, since they are far less intense than the input lanes.
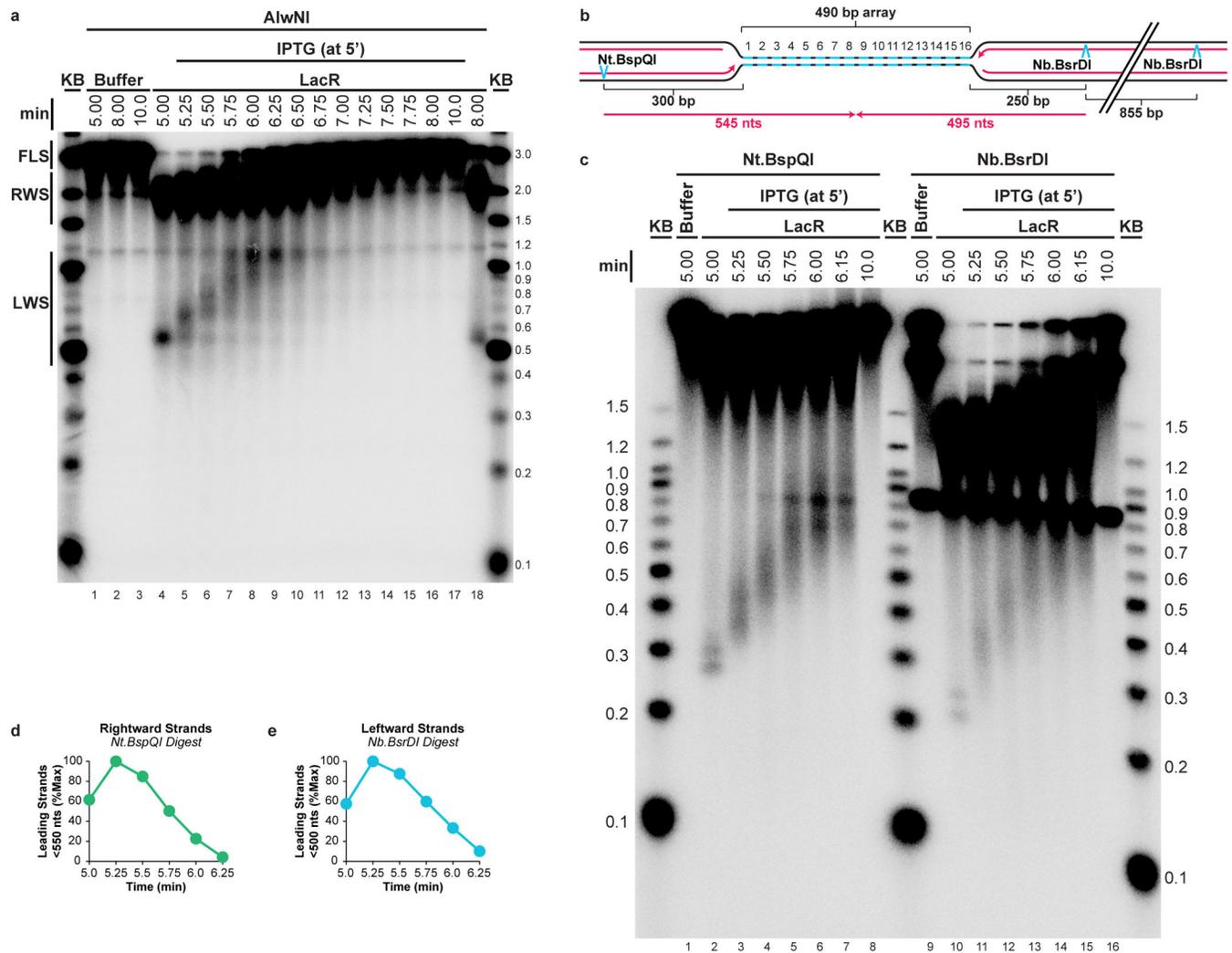
Extended Data
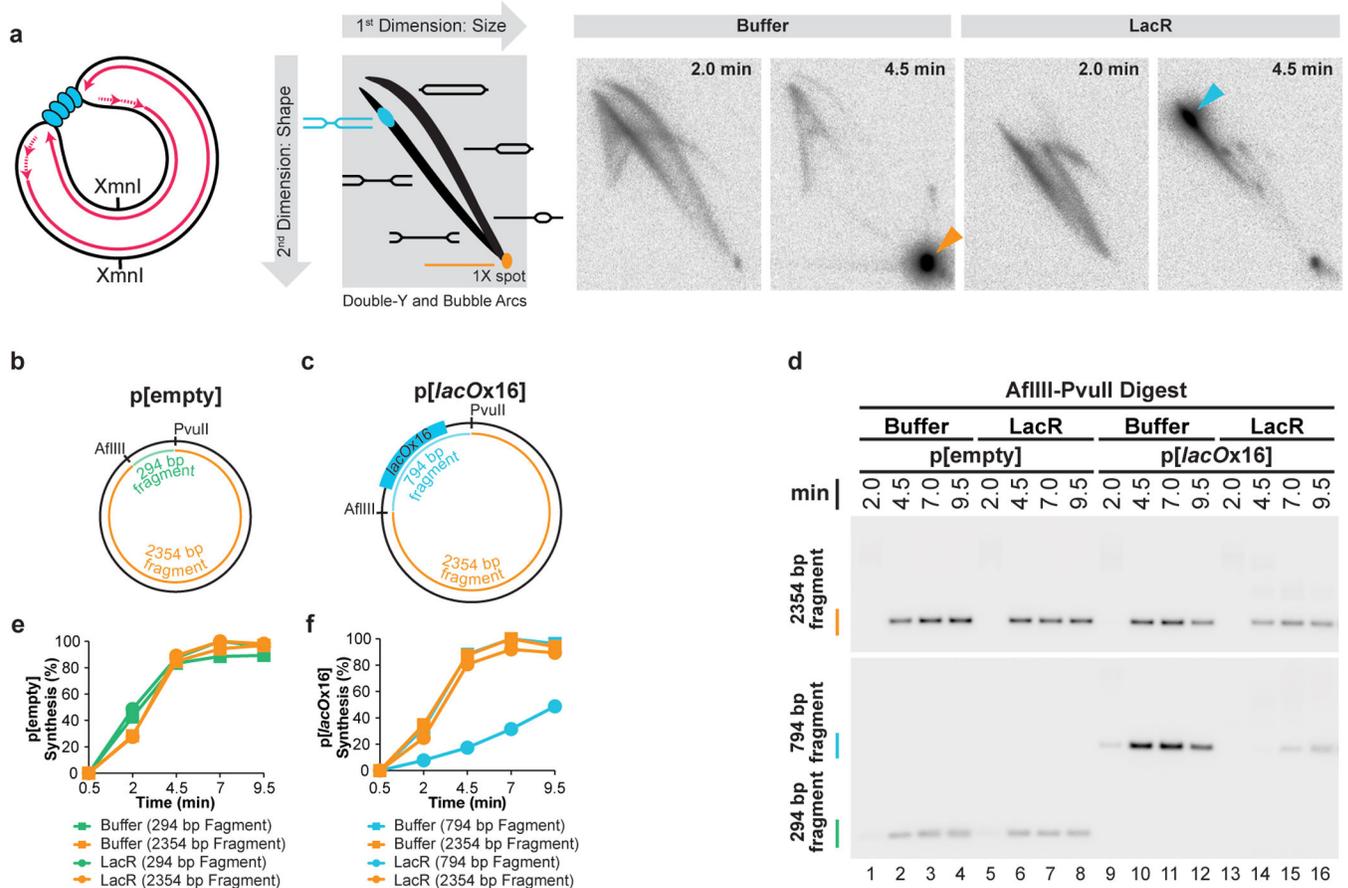
Extended Data Figure 1. Sequence-specific termination can be induced at a LacR array

(**A**) To investigate whether a LacR array blocks replication forks, a plasmid containing a tandem array of 16 *lac* operator (*lacO*) sequences, p[*lacO*x16], was incubated with buffer or LacR and then replicated in egg extract containing [α-^{32}P]dATP. Radiolabelled replication intermediates were cleaved with XmnI (far left cartoon) and separated according to size and shape by 2-dimensional gel electrophoresis (see schematic of 2-D gel). As replication neared completion at 4.5 minutes, mainly linear molecules were produced in the presence of buffer (orange arrowhead). In contrast, in the presence of LacR, a discrete spot appeared on the Double Y arc (blue arrowhead), demonstrating that converging replication forks accumulate

at a specific locus on p[*lacO*x16]. These data indicate that 16 copies of LacR block replication forks.

(B–F) To test whether the double-Y structures observed in (A) arose from replication forks stalling at the outer edges of the *lacO* array, we tested whether LacR specifically inhibited replication of *lacO* sequences. To this end, p[*lacOx16*] (C) and the parental plasmid lacking *lacO* repeats, p[*empty*] (B), were incubated in the presence of buffer or LacR and replicated using *Xenopus* egg extracts containing [α-^{32}P]dATP. Radiolabelled replication intermediates were cleaved with AflIII and PvuII to release the 2354 bp plasmid backbone (B and C) and a 294 bp control fragment from p[*empty*] (B) or a 794 bp *lacO* fragment from p[*lacO*x16] (C). The plasmid backbone and the respective inserts were separated on a native gel and detected by autoradiography (D). A longer exposure of the small fragments is shown, since they are less intense than the large fragments. The results in panel (D) were quantified in (E) and (F). Importantly, LacR specifically inhibited replication of the *lacO*-containing fragment in p[*lacO*x16] (F, blue circles) but not the control fragment in p[*empty*] (E, green circles). We conclude that LacR prevents replication of the *lacO* array and that the double-Y's in (A) represent forks converged on the outer edges of the array. Importantly, synthesis within the 2354 bp backbone fragment (F, orange circles) of p[*lacO*x16] was not inhibited in the presence of LacR, indicating that no global structural changes occur that inhibit replication.

Extended Data Figure 2. Supplemental fork progression data

(A) The gel shown in Figure 1E was overexposed and shown in its entirety so that the smaller leftward strands (LWS, Fig 1D) could be detected. As observed for the rightward strands (RWS, Fig 1E), LWS rapidly increased in size and then disappeared as they were ligated to produce full length strands (FLS, Fig 1E).

(B–E) To determine whether the heterogeneity of LWS (A) and RWS (Fig 1E) was due to delayed extension of lagging strands, or because a significant fraction of leading strands did not restart upon IPTG addition, we specifically monitored leading strand progression upon IPTG addition on p[*lacO*x16]. To this end, DNA samples were treated with Nt.BspQI or Nb.BsrDI to specifically liberate the rightward or leftward leading strands, respectively (B), and DNAs were separated on a denaturing agarose gel (C). Prior to IPTG addition, discrete leading strand products of the expected size were observed (lanes 2 and 10). The presence of two stall products reflects the fact that at a slow rate, the replisome bypasses LacR (see also Fig 3). Upon IPTG addition, these species rapidly and completely shifted up the gel, indicating that rightward and leftward leading strands restarted efficiently. Therefore, the heterogeneity of the LWS (A) and RWS (Fig. 1E) is probably due to delayed ligation of a

new Okazaki fragment to the lagging strands. Quantification of leading strands that had not reached the midpoint of the array (rightward and leftward strands smaller than 550 and 500 nts, respectively, B) revealed that by 6.25 minutes, 90% of rightward and leftward leading strands passed the midpoint of the array (D–E). This demonstrates that leading strands pass each other when forks meet.
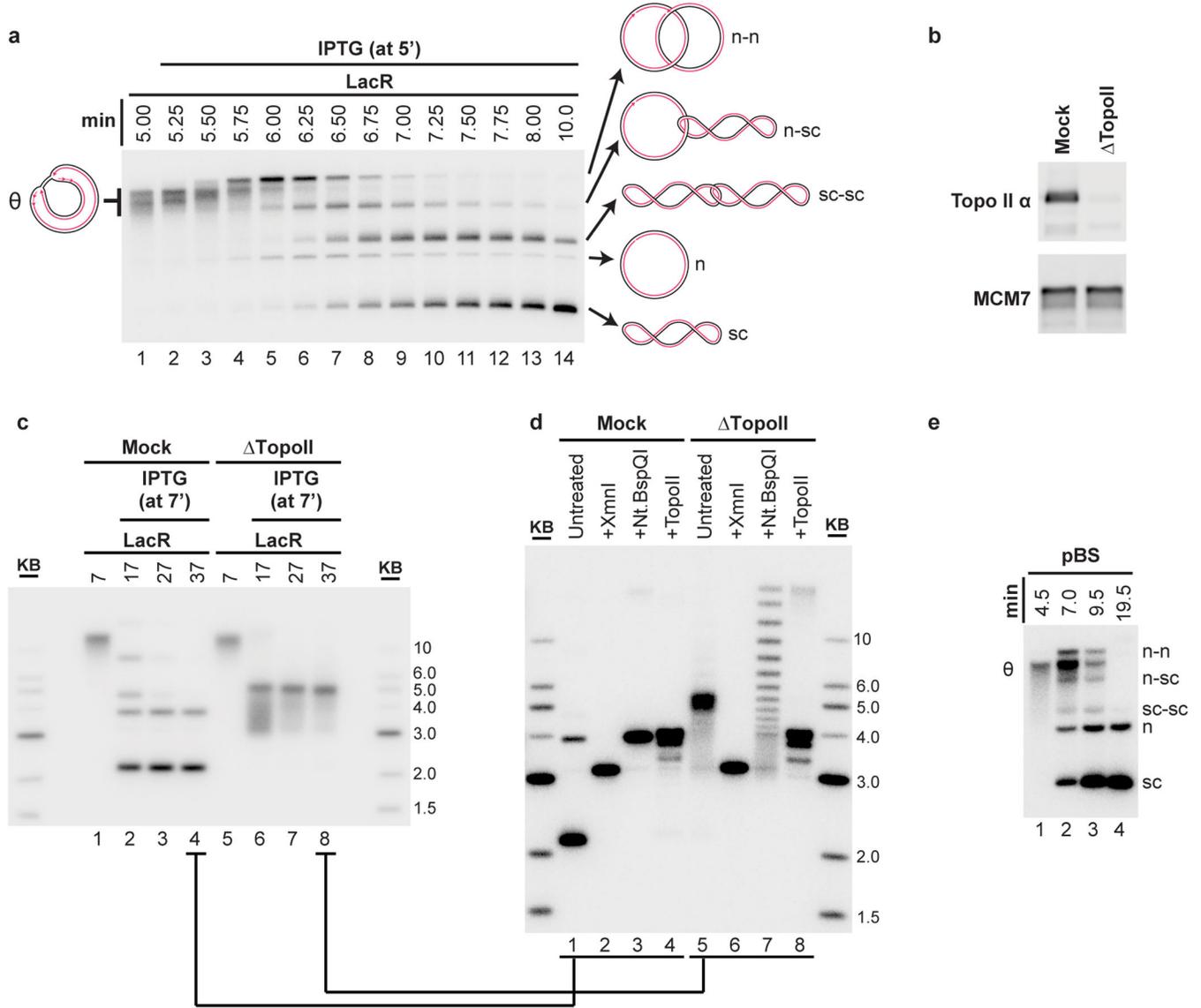

Extended Data Figure 3. Topo II-dependent decatenation of p[lacOx16]
(A) The autoradiograph in primary Figure 1G is reproduced with cartoons indicating the structures of the replication and termination intermediates n-n, n-sc, sc-sc, n, and sc (see main text for definitions). The order of appearance of the different catenanes matches previous work[5] (n-n, then n-sc, then sc-sc).
(B–D) To determine the role of Topo II during termination within a *lacO* array, termination was monitored in mock- or Topo II-depleted extracts. To confirm immunodepletion of Topo II, Mock and Topo II-depleted NPE was blotted with MCM7 and Topo II antibodies (B).

p[*lacO*x16] was incubated with LacR, then replicated in either mock- or Topo II-depleted egg extracts in the presence of [α-^{32}P]dATP, and termination was induced with IPTG (at 7'). Untreated DNA intermediates were separated by native gel electrophoresis (C). In the mock-depleted extract, nicked and supercoiled monomers were readily produced (as in (A), albeit with slower kinetics due to nonspecific inhibition of the extracts by the immunodepletion procedure), while in the Topo II-depleted extracts, a discrete species was produced. DNA from the last time point in each reaction (lanes 4 and 8 in (C)) was purified and treated with XmnI, which cuts p[*lacO*x16] once, or Nt.BspQI, which nicks p[*lacO*x16] once, or recombinant Topo II, and then separated by native gel electrophoresis (D). Cleavage of the mock- and TopoII-depleted products with XmnI yielded the expected linear 3.15 kb band (lanes 2 and 6), demonstrating that in both extracts, all products were fully dissolved topoisomers of each other. Relaxation of the mock-depleted products by nicking with Nt.BspQI yielded a discrete band corresponding to nicked plasmid (lane 3), while the TopoII-depleted products were converted to a ladder of discrete topoisomers (lane 7), which we infer represent catenated dimers of different linking numbers, since the mobility difference cannot be due to differences in supercoiling. Importantly, the mobility shift following Nt.BspQI treatment (lane 5 vs lane 7) demonstrated that the Topo II-depleted products (lane 5) were covalently closed and thus in the absence of Topo II ligation of the daughter strands still occurred. Treatment of the mock- and Topo II-depleted products with recombinant human Topo II produced the same relaxed monomeric species (lanes 4 and 8), further confirming that the Topo II-depleted products contained catenanes. Collectively, these observations demonstrate that termination within a *lacO* array in Topo II depleted extracts produces highly catenated supercoiled-supercoiled dimers, as seen in cells lacking Topo II[16,17]. These data confirm that Topo II is responsible for decatenation and argue that termination within a *lacO* array reflects physiological termination.

(E) n-n, n-sc, sc-sc, n, and sc products were also detected when plasmid lacking *lacO* sequences (pBlueScript) was replicated in the absence of LacR without the use of Cyclin A to synchronize replication. Therefore, these intermediates arise in the course of unperturbed DNA replication in *Xenopus* egg extracts.
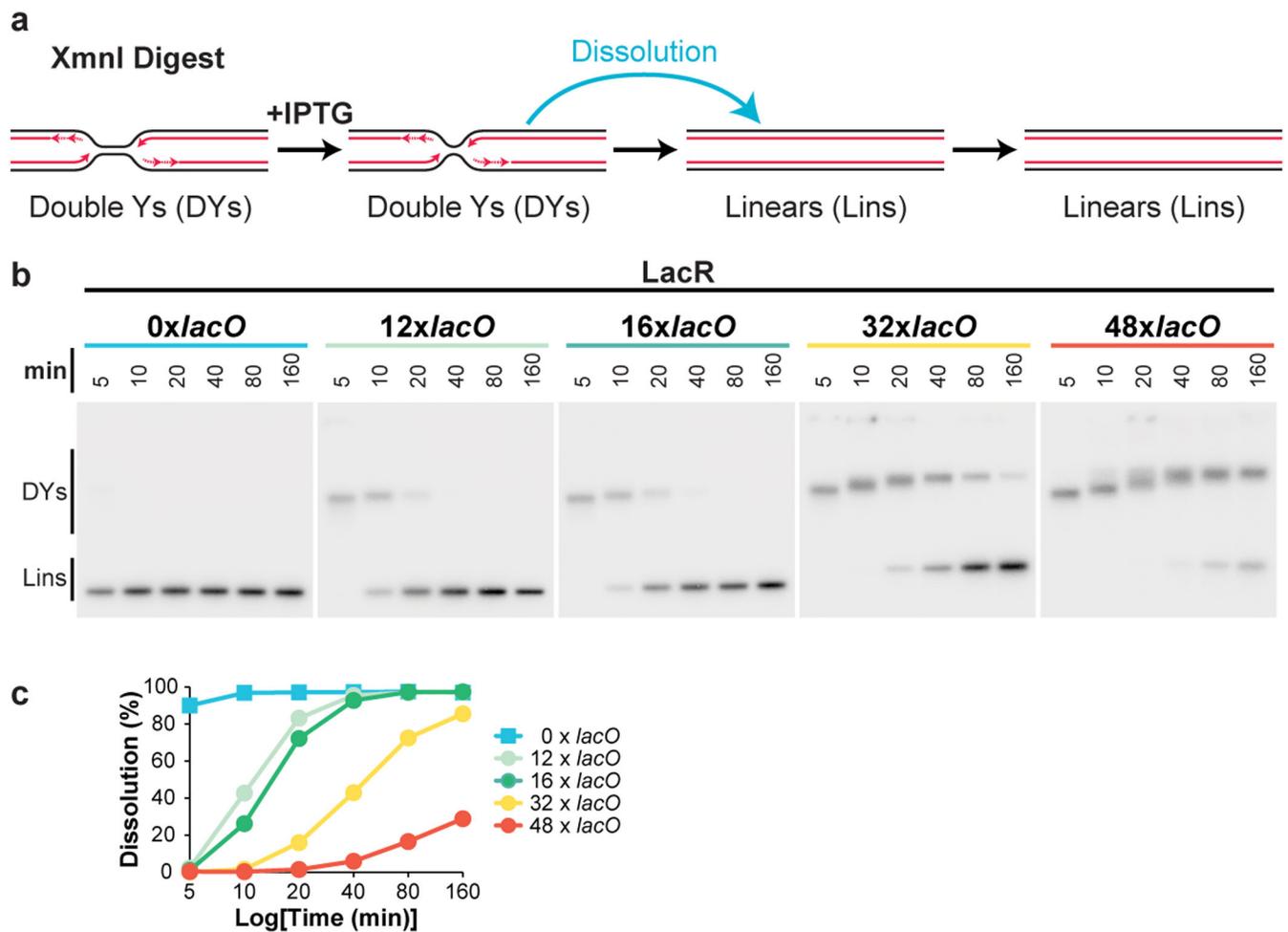
Extended Data Figure 4. Inhibition of termination by different size LacR arrays

(**A**) Cartoon depicting intermediates detected in the dissolution assay.

(**B**) To determine the ability of different-sized LacR arrays to inhibit termination, the earliest stage of termination, *dissolution* (A), was monitored in plasmids containing 0, 12, 16, 32, or 48 *lacO* repeats. Plasmids were incubated with LacR, and replicated in the presence of [α-^{32}P]dATP. To measure *dissolution*, radiolabelled termination intermediates were cut with XmnI. Cleaved products were separated on a native agarose gel and detected by autoradiography.

(**C**) Quantification of dissolution in (B). When 12 or more *lacO* repeats were present in the array, dissolution was robustly inhibited for at least 5 minutes. Potent inhibition lasted 10 minutes when 32 *lacO* sequences were present, and 20 minutes in the presence of 48 *lacO* sequences. In the absence of *lacO* sequences, dissolution was essentially complete by 5 minutes. Therefore, 12 *lacO* repeats are sufficient to inhibit termination for 5 minutes.
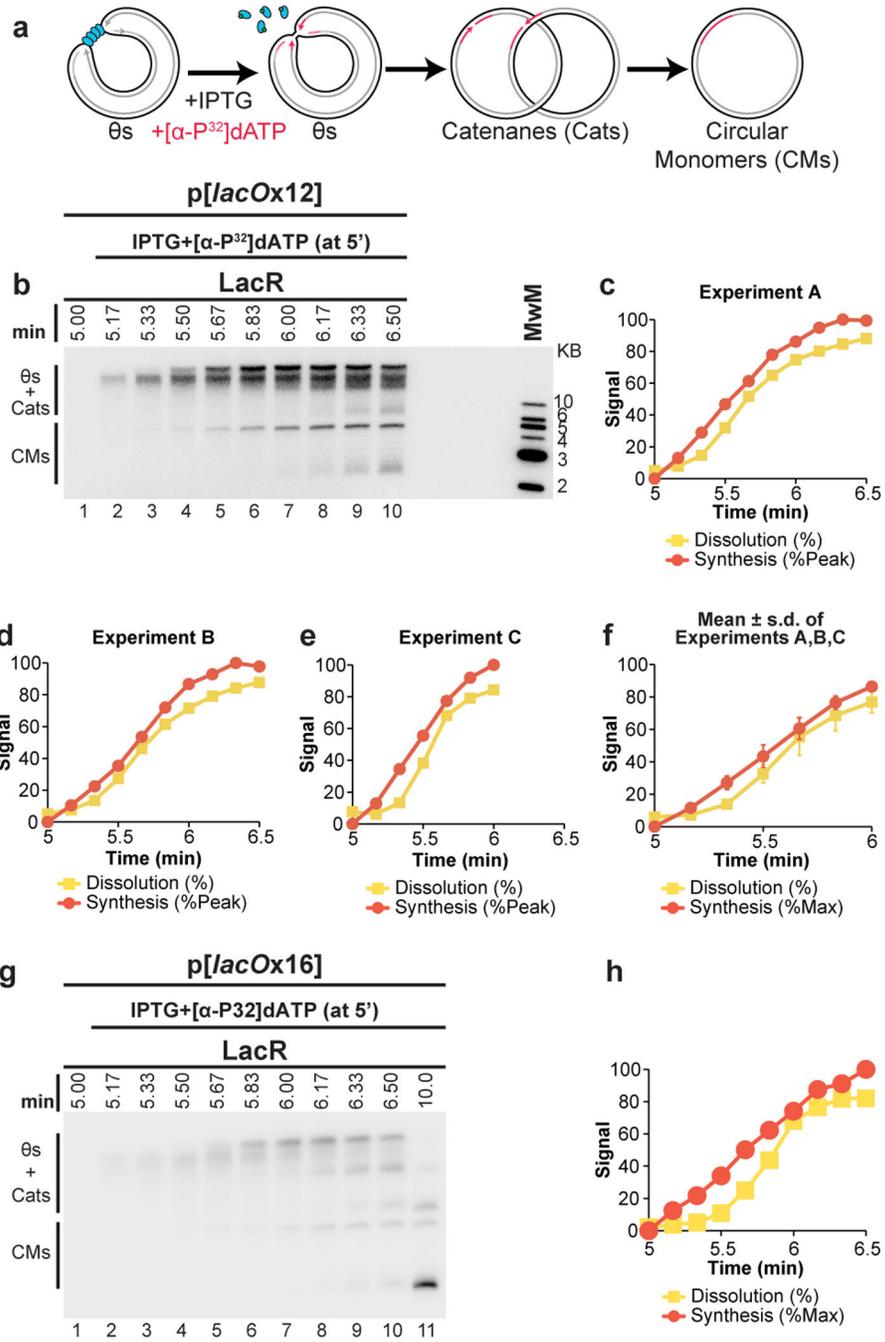
Extended Data Figure 5. The rate of total DNA synthesis does not slow before dissolution
(A–C) To further test whether replication stalls or slows prior to dissolution, p[*lacO*x12] was pre-incubated with LacR and replicated in *Xenopus* egg extracts. Termination was then induced by addition of IPTG after 5 minutes. Simultaneously, [α-32P]dATP was added to specifically radiolabel DNA synthesized following IPTG addition (A). Radiolabelled DNA was then separated on a native agarose gel and total signal was measured by autoradiography (B). Total signal was quantified, normalized to peak signal, and graphed alongside the rate of dissolution, which was also measured in the same experiment (C). This

approach gives a highly sensitive measure of DNA synthesis without manipulation of DNA samples. DNA synthesis should occur primarily within the *lacO* array (see Extended Data Fig. 1). Upon IPTG addition, there was an approximately linear increase in signal, which plateaued by 5.83 min. Importantly, dissolution was 65% complete by 5.83 min. Therefore, the large majority of dissolution occurs without stalling of DNA synthesis.

(D–E) Experimental repeats of (B–C)

(F) The experiments shown in (C–E) were graphed together with mean±s.d. Synthesis data was normalized so that for each experiment, synthesis at 1 min was assigned a value of 84.4%, since this was the average value from (C–D), where synthesis was allowed to plateau. Given the rate of replication fork progression in these egg extracts (260 bp/minute[32]) and the size of the array (365 bp), forks should require, on average, 0.7 minutes to converge if no stalling occurs (365 bp ÷ 2 ÷ 260 bp/min = 0.7 min). The time required for dissolution was not appreciably longer than this (dissolution was 50% complete by 0.67 min after IPTG addition, (F)), consistent with a lack of stalling.

(G–H) The experiment shown in (B–C) was repeated using p[*lacO*x16]. Synthesis was approximately linear until 6.17 minutes, at which point 81% of molecules had dissolved, further demonstrating that the majority of dissolution occurs without stalling of DNA synthesis.
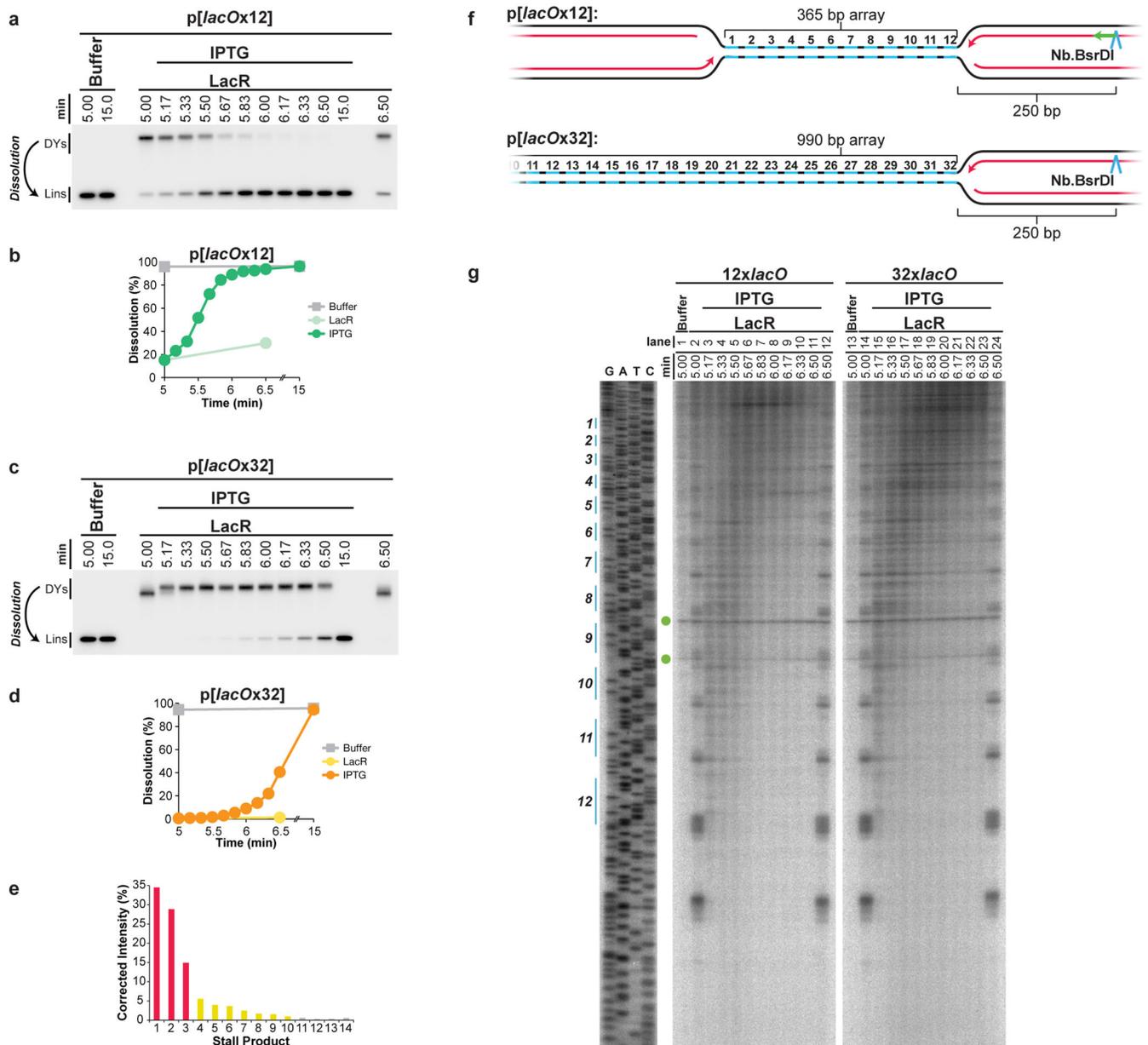
Extended Data Figure 6. Replisome progression through 12x and 32x lacO arrays

(A–D) To test whether replisomes meet later in a *lacO*x32 array than *a lacO*x12 array, we monitored dissolution. LacR Block-IPTG release was performed on p[*lacO*x12] and p[*lacO*x32] and radiolabelled termination intermediates were digested with XmnI to monitor the conversion of double-Y molecules to linear molecules (Dissolution). Cleaved molecules were separated on a native agarose gel, detected by autoradiography (A,C), and quantified (B,D). Upon IPTG addition, dissolution was delayed by at least 1 minute within the 32x*lacO* array compared to the 12x*lacO* array (B,D). Moreover, by 6 minutes, 92% of forks had undergone dissolution on p[*lacO*x12] while only 9% had dissolved on p[*lacO*x32] (B,D). **(E)** Stall products within the 12x*lacO* array (Fig. 3B, Lane 2) were quantified, signal was corrected based on size differences of the products, and the percentage of stall products at

each stall point was calculated. 78% of leading strands stalled at the first three arrest points (red columns), 19% stalled at the fourth to tenth arrest points (yellow columns) and the remaining 3% stalled at the tenth to fourteenth arrest points (grey columns). The appearance of fourteen arrest points reproducible and surprising, given that the presence of only twelve *lacO* sequences was confirmed by sequencing in the very preparation of p[*lacO*x12] that was used in Fig. 3. The thirteenth and fourteenth arrest points cannot stem from cryptic *lacO* sites beyond the twelfth *lacO* site, as this would position the first *leftward* leading strand stall product ∼90 nucleotides from the *lacO* array, instead of the observed ∼30 nucleotides (see **F-G**). At present, we do not understand the origin of these stall products.

(F–G) Progression of *leftward* leading strands into the array. The same DNA samples used in Fig. 3 were digested with the nicking enzyme Nb.BsrDI, which released leftward leading strands (F), and separated on a denaturing polyacrylamide gel (G). The *lacO* sites of p[*lacO*x12] are highlighted in blue on the sequencing ladder (G), which was generated using the primer JDO109 (Green arrow, F). Green circles indicate two non-specific products of digestion. These products arise because nicking enzyme activity varies between experiments, even under the same conditions. There was no significant difference in the pattern of *leftward* leading strand progression between the 12x*lacO* and 32x*lacO* arrays, as seen for the *rightward* leading strands (Fig. 3B). Specifically, by 5.67 minutes, the majority of leading strands had extended beyond the seventh *lacO* repeat within *lacO*x12 (lane 6) and the equivalent region of *lacO*x32 (lane 18). Therefore, progression of leftward leading strands is unaffected by the presence of an opposing replisome, suggesting that converging replisomes do not stall when they meet.
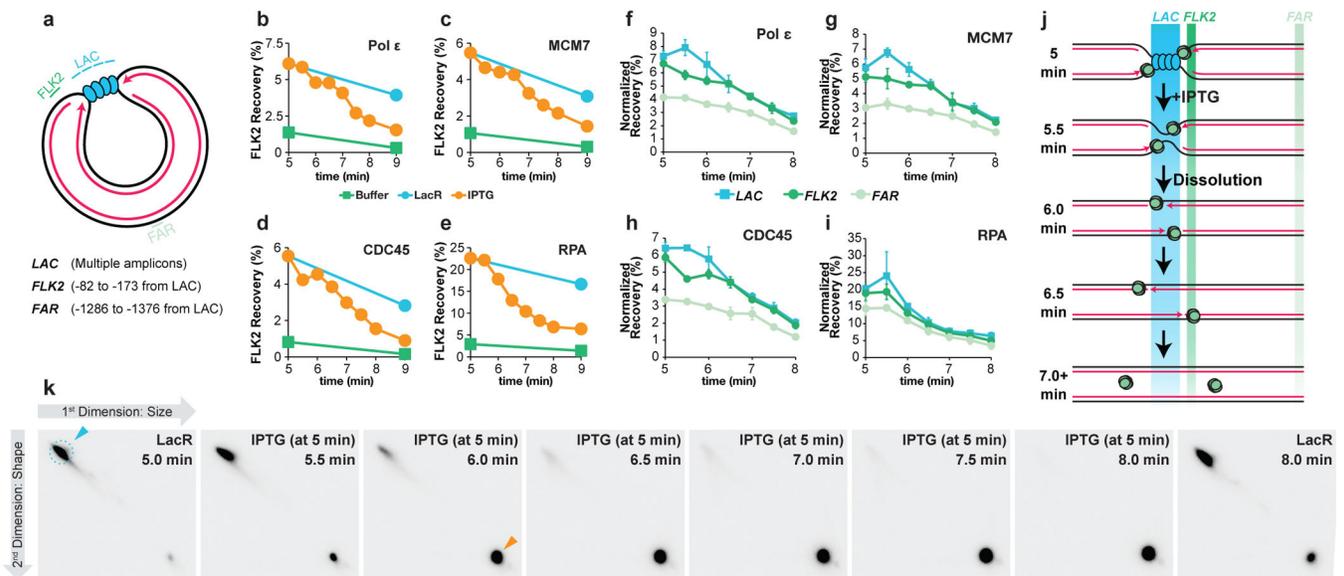
Extended Data Figure 7. Supplemental ChIP data
(A) Cartoon depicting the *LAC, FLK2* and *FAR* loci, which were used for ChIP. Their precise locations relative to the leftward edge of the *lacO* array are indicated. The *LAC* amplicon is present in four copies distributed across the *lacOx16* array and three copies distributed across the *lacOx12* array.

(B–E) p[*lacO*x12] was incubated with buffer or LacR and termination was induced at 5 minutes by IPTG addition. MCM7, RPA, CDC45, and Polε ChIP was performed at different time points after IPTG addition but also in the buffer control and no IPTG control. Recovery of *FLK2* was measured as a percentage of input DNA. Upon IPTG addition, ChIP signal declined and by 9 minutes was comparable to the buffer control, demonstrating that unloading of replisomes was induced within 4 minutes of IPTG addition.

(F) To test whether movement of the replisome into and out of the *lacO* array could be detected upon IPTG addition, termination was monitored within a *lacO* array, and we performed ChIP of the leading strand polymerase Polε, which was inferred to move into and out of the array based on the behavior of leading strands during termination (Extended Data Fig 2B–E). It was predicted that Polε ChIP at the *LAC* locus should increase slightly as Polε enters the *lacO* array and decline again as converging polymerases pass each other, but persist at *FLK2* while the polymerases move out of the array. Prior to IPTG addition, Polε was enriched at *LAC* and *FLK2* compared to *FAR*, consistent with the leading strands being positioned on either side of the *lacO* array (Extended Data Fig 2C, Fig. 3). Upon IPTG addition, Polε became modestly enriched at *LAC* compared to *FLK2* (5.5 min) but then declined to similar levels at both *LAC* and *FLK2* by 6.5 min. These data are consistent with the leading strand polymerases entering the *lacO* array and passing each other.

(G–H) To test whether CMG exhibited the same ChIP profile as Polε, MCM7 and CDC45 ChIP was performed using the same samples. Following IPTG addition, MCM7 and CDC45 were enriched at *LAC* compared to *FLK2* (5.5 min), then declined to similar levels at both *LAC* and *FLK2* by 6.5 min, as seen for Polε (F). These data are consistent with a model in which CMGs enter the array and pass each other during termination. A caveat of these experiments is the relatively high recovery of the *FAR* locus in MCM7, CDC45, and Polε ChIP. Specifically, signal was at most only ∼2-fold enriched at *LAC* compared to *FAR*. This was not due to high background binding, because by the end of the experiment (10 minute time point, not shown), we observed a decrease in signal of ∼5–7 fold. Furthermore, we observed ∼5–7 fold enrichment in binding (ChIP) of replisome components to p[*lacO*x12] that had been incubated in LacR compared to a buffer control (see G-I, below). Instead, the high *FAR* signal was likely due to poor spatial resolution of the ChIP. Consistent with this, when a plasmid containing a DNA interstrand cross-link (ICL) was replicated, essentially all replisomes converged upon the ICL but the ChIP signal for MCM7 and CDC45 was only ∼3–4 fold enriched at the ICL compared to a control locus[41]. We speculate that the higher background observed at the control locus in our experiments is due to the decreased distance of the control locus from the experimental locus (1.3 kb for p[*lacO*x16] and p[*lacO*x12] vs. 2.4 kb for the ICL plasmid) and possibly due to increased catenation of the parental strands during termination. The high signal at *FAR* should not complicate interpretation of the MCM7, CDC45 and Polε ChIP (F), as signal at *FAR* was essentially unaltered between 5 and 6.5 minutes. Further evidence that the high signal seen at the *FAR* locus emanates from forks stalled near the *lacO* array is presented in panel (*K*).

(I) ChIP of RPA was performed on the same chromatin samples used in B-D. As seen for pol ε, MCM7, and CDC45, enrichment of RPA at *LAC* compared to *FAR* was relatively low, consistent with poor spatial resolution.

(J) Predicted binding of CMGs to the *LAC, FLK2* and *FAR* loci before and after IPTG addition if CMGs converging CMG pass each other.

(K) To determine whether most forks stalled at the array and not elsewhere in the plasmid, we performed a time course in which p[*lacO*x16] undergoing termination was examined by 2-dimensional gel electrophoresis (2-D gel) at various time points. p[*lacO*x16] was pre-bound to LacR and replicated in *Xenopus* egg extract containing [α-^{32}P]dATP. Termination was induced by IPTG addition and samples were withdrawn at different times. Radiolabelled replication intermediates were cleaved with XmnI (as in Extended Data Fig. 1A) and separated according to size and shape on 2-D gels[50]. A parallel reaction was performed in which samples were analyzed by ChIP, which was one of the repeats analyzed in (B)-(E). In the presence of LacR, a subset of Double Y molecules accumulated (blue arrowhead), demonstrating that 83% of replication intermediates (signal in dashed blue circle) contained two forks converged at a specific locus. Following IPTG addition, linear molecules rapidly accumulated (orange arrow) as dissolution occurred. Importantly, the vast majority of signal was present in the discrete double-Y and linear species (blue and orange arrows), demonstrating that the relatively high ChIP signal observed at *FAR* in panels F-I was derived from forks present at the *lacO*x16 array and not elsewhere.
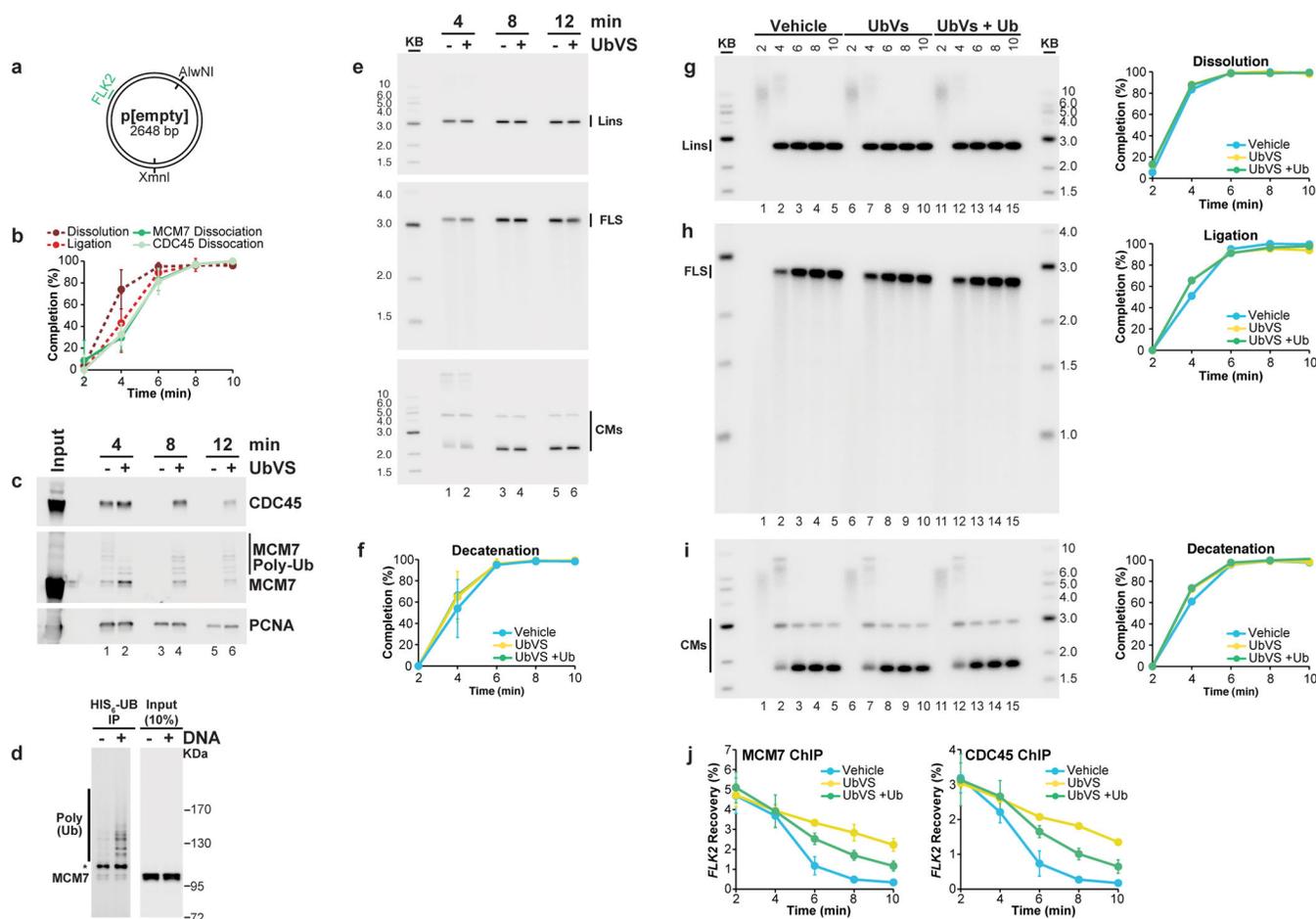
Extended Data Figure 8. Supplemental termination data for p[empty] experiments
(A) Cartoon depicting the XmnI and AlwNI sites on p[*empty*], which are used for the dissolution and ligation assays, respectively, and the *FLK2* locus, which is used for ChIP.

(B) Plasmid DNA without a *lacO* array (p[*empty*]) was replicated and at different times chromatin was subjected to MCM7 and CDC45 ChIP. Percent recovery of *FLK2* was quantified and used to measure dissociation of MCM7 and CDC45 (see methods). Dissolution and ligation were also quantified in parallel. mean±s.d. is plotted (n=3). The MCM7 and CDC45 dissociation data is obtained from the vehicle controls in Figure 5B–C, while the dissolution and ligation data are obtained from the vehicle controls in Fig 5D–E.

(C) To seek independent evidence for the conclusions of the ChIP data presented in Figure 5B–C, we used a plasmid pull-down procedure. p[empty] was replicated in egg extracts treated with Vehicle or Ub-VS. At the indicated times, chromatin-associated proteins were captured on LacR-coated beads (which binds DNA independently of *lacO* sites) and analyzed by Western blotting for CDC45, MCM7, and PCNA. CDC45 and MCM7 dissociated from chromatin by 8' in the vehicle control, but persisted following UbVS treatment.

(D) To test whether the MCM7 modifications detected in panel (C) represented ubiquitylation, extracts were incubated with HIS_6-Ubiquitin in the absence of Cyclin A, and in the absence or presence of plasmid DNA. After 15 minutes, HIS_6-tagged proteins were captured by nickel resin pull down and blotted for MCM7. DNA replication greatly increased the levels of ubiquitylated MCM7, with the exception of a single species that was ubiquitylated independently of DNA replication (*). These data show that MCM7 is ubiquitylated during plasmid replication in egg extracts, as observed in yeast and during replication of sperm chromatin following nuclear assembly in egg extracts[24,25].

(E) In parallel to the plasmid pull-downs performed in (C), DNA samples were withdrawn for dissolution, ligation, and decatenation assays, none of which were perturbed by UbVS treatment. These data support our conclusion, based on ChIP experiments (Fig. 5), that defective CMG unloading does not affect dissolution, ligation, or decatenation.

(F) Decatenation was measured in the same reactions used to measure Dissolution and Ligation (Fig. 5D–E), mean±s.d. is plotted (n=3).

(G–I) Given the experimental variability at the 4 minute time point in Figures 5D–F, the primary data and quantification for dissolution (G), ligation (H), and decatenation (I) for one of the three experiments summarized in Figure 5D–F is presented. This reveals that Ub-VS does not inhibit dissolution, ligation, or decatenation at the 4 minute time point. The same conclusion applies to two additional repetitions of this experiment (data not shown).

(J) The primary ChIP data used to measure dissociation of MCM7 and CDC45 in Fig 5B–C is shown. Recovery of *FLK2* was measured. mean±s.d. is plotted (n=3).

A.

Plasmid	Insert	Construction
pJD82	SacI-BsrGI-(lacO)x4-BsiWI-KpnI	Replacement of the sequence between SacI and KpnI of pBluescript II KS-
pJD85	SacI-BsrGI-(lacO)x8-BsiWI-KpnI	JDO38/39 annealed and cloned into pJD82 that had been cut with BsrGI
pJD88	SacI-BsrGI-(lacO)x16-BsiWI-KpnI	BsrGI/BsiWI fragment from pJD85 cloned into pJD85 that had been cut with BsrGI
pJD92	SacI-BsrGI-(lacO)x32-BsiWI-KpnI	BsrGI/BsiWI fragment from pJD88 cloned into pJD88 that had been cut with BsrGI
pJD100	SacI-BsrGI-(lacO)x48-BsiWI-KpnI	BsrGI/BsiWI fragment from pJD88 cloned into pJD92 that had been cut with BsrGI
pJD104	SacI-BsrGI-(lacO)x12-BsiWI-KpnI	JDO38/39 annealed and cloned into pJD85 that had been cut with BsrGI
pJD105	SacI-Nb.BsmI-BsiWI-Nt.BbvCI-KpnI	Replacement of the sequence between SacI and KpnI of pBluescript II KS- with JDO42/43
pJD139	SacI-Nb.BsmI-BsiWI-Nt.BbvCI-KpnI	Quickchange mutagenesis of pJD105 using JDO94/95
pJD145	SacI-Nb.BsmI-BsiWI-Nt.BbvCI-KpnI	Quickchange mutagenesis of pJD139 using JDO100/10
pJD150	SacI-Nb.BsmI-(lacO)x12-BsiWI-Nt.BbvCI-KpnI	BsrGI/BsiWI fragment from pJD104 cloned into pJD145 that had been cut with BsiWI
pJD152	SacI-Nb.BsmI-(lacO)x16-BsiWI-Nt.BbvCI-KpnI	BsrGI/BsiWI fragment from pJD88 cloned into pJD145 that had been cut with BsiWI
pJD156	SacI-Nb.BsmI-(lacO)x32-BsiWI-Nt.BbvCI-KpnI	BsrGI/BsiWI fragment from pJD92 cloned into pJD145 that had been cut with BsiWI
pQNT	-	pCDFDuet-1 containing a HincII site (pQuant from [41])

B.

Oligo	Sequence	Description
JDO38	5'-GTACATCAATTGTGAGCGGATAACAATTGTTAGGGAGGAATTGTGAGCGGATAACAATTTGGAGTTGATAATTGTGAGCGGATAACAATTGGCTTCAACGTAATTGTGAGCGGATAACAATTTCC-3'	Can be annealed to JDO39 to generate dsDNA containing 4x lacO sites with ends that are compatible with BsiWI and BsrGI.
JDO39	5'-GTACGGAAATTGTTATCCGCTCACAATTACGTTGAAGCCAATTGTTATCCGCTCACAATTATCAACTCCAAATTGTTATCCGCTCACAATTCCTCCCTAACAATTGTTATCCGCTCACAATTGAT-3'	Can be annealed to JDO38 to generate dsDNA containing 4x lacO sites with ends that are compatible with BsiWI and BsrGI.
JDO42	5'-CTGTACAGCATTCCCATGGCGTACGTTCTAGACCTCAGCTATGGTACC-3'	Can be annealed to JDO43 to generate dsDNA containing sites for BsrGI-Nb.BsmI-NcoI-BsiWI-XbaI-Nb.BbvCI with ends that are compatible with SacI and KpnI.
JDO43	5'-AGCGGTACCATAGCTGAGGTCTAGAACGTACGCCATGGGAATGCTGTACAGAGCT-3'	Can be annealed to JDO42 to generate dsDNA containing sites for BsrGI-Nb.BsmI-NcoI-BsiWI-XbaI-Nb.BbvCI with ends that are compatible with SacI and KpnI.
JDO94	5'-TAAGGGATTTTGCCGATTTCGGCCTATGCTCTTCGCAGTGTGGTTAAAAAATGAGC-3'	Used with JDO95 to introduce Nt.BspQI and Nb.BtsI sites upstream of Nb.BsmI in pJD105-derived plasmids by Quickchange mutagenesis.
JDO95	5'-GCTCATTTTTTAACCACACTGCGAAGAGCATAGGCCGAAATCGGCAAAATCCCTTA-3'	Used with JDO94 to introduce Nt.BspQI and Nb.BtsI sites upstream of Nb.BsmI in pJD105-derived plasmids by Quickchange mutagenesis.
JDO100	5'-TGAGCGTCGATTCATTGCTTTGTGATGCTCGTCAGGGGG-3'	Used with JDO101 to introduce Nb.BsrDI site downstream of BbvCI in pJD105-derived plasmids by Quickchange mutagenesis.
JDO101	5'-CCCCCTGACGAGCATCACAAAGCAATGAATCGACGCTCA-3'	Used with JDO100 to introduce Nb.BsrDI site downstream of BbvCI in pJD105-derived plasmids by Quickchange mutagenesis.
JDO107	5'-CAGTGTGGTTAAAAAATGAGCTG-3'	Sequencing primer for mapping leading strands released by Nt.BspQI digestion
JDO109	5'-CATTGCTTTGTGATGCTCGT-3'	Sequencing primer for mapping leading strands released by Nb.BsrDI digestion
JDO110	5'-TGGTTAAAAAATGAGCTGATTTAACA-3'	Sequencing primer for mapping lagging strands released Nb.BtsI digestion.
JDO111	5'-TGAGGTCTAGAACGTACGGAAA-3'	Sequencing primer for mapping leading strands released by Nb.BbvCI digestion.
FLK2_F	5'-TCTTCGCTATTACGCCAGCT-3'	Used with FLK2_R to amplify the region 82-173 bases upstream of the lacO array in pJD152
FLK2_R	5'-TTACAACGTCGTGACTGGGA-3'	Used with FLK2_F to amplify the region 82-173 bases upstream of the lacO array in pJD152
LAC_F	5'-AGCGGATAACAATTGTTAGGGA-3'	Used with LAC_R to amplify four sites within the lacO array in pJD152
LAC_R	5'-CTCACAATTACGTTGAAGCCAA-3'	Used with LAC_F to amplify four sites within the lacO array in pJD152
FAR_F	5'-ATTGCTACAGGCATCGTGGT-3'	Used with FAR_R to amplify the region 1286-1375 bases upstream of the lacO array in pJD152
FAR_R	5'-GGGATCATGTAACTCGCCTTGA-3'	Used with FAR_F to amplify the region 1286-1375 bases upstream of the lacO array in pJD152
QNT_F	5'-TACAAATGTACGGCCAGCAA-3'	Used with QNT_R to amplify pQNT
QNT_R	5'-GAGTATGAGGGAAGCGGTGA-3'	Used with QNT_F to amplify pQNT

Extended Data Figure 9. Tables of plasmids and oligonucleotides used
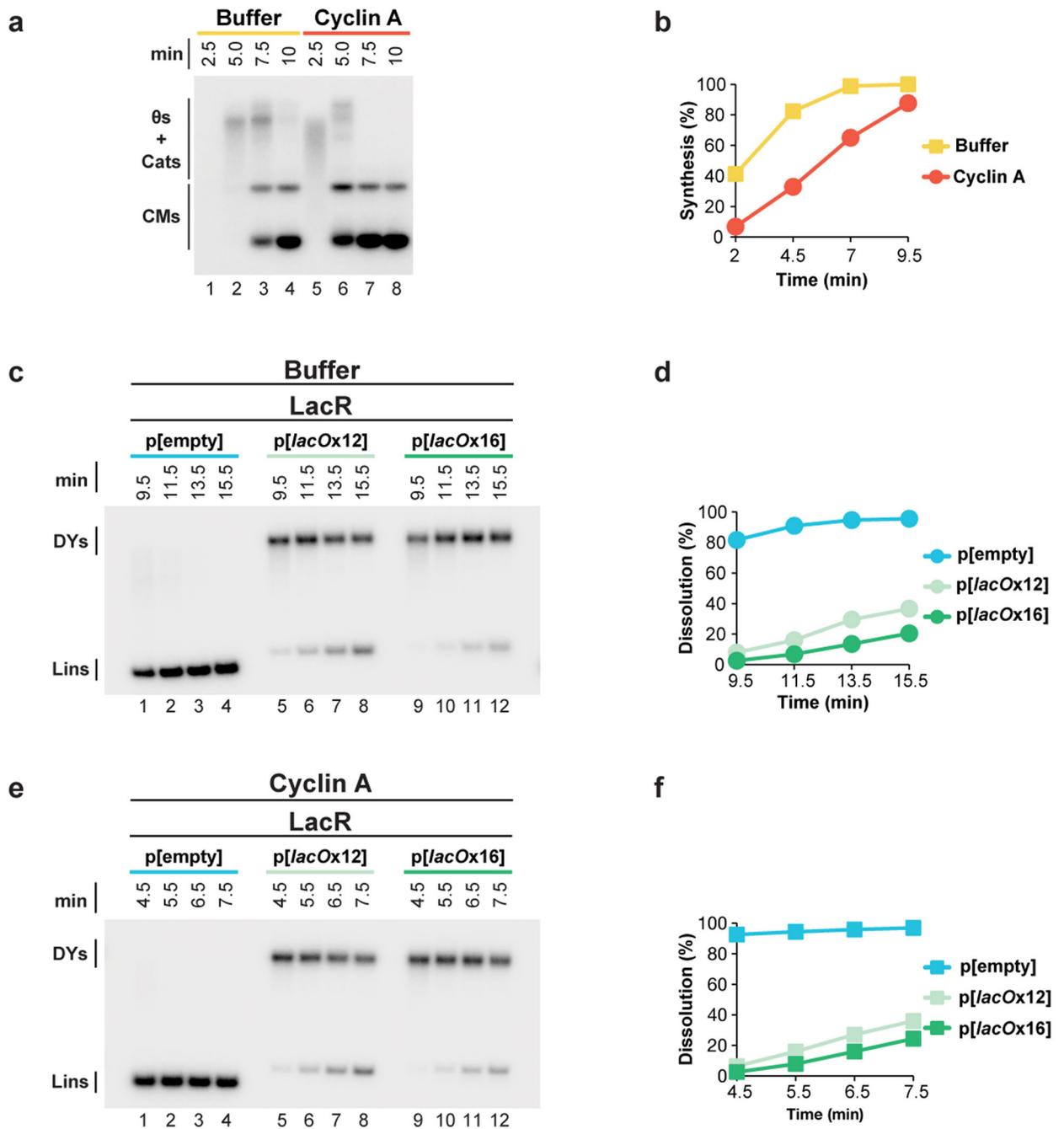
Extended Data Figure 10. Cyclin A treatment synchronizes DNA replication in Xenopus egg extracts

(A–B) To synchronize DNA replication in Xenopus egg extracts, we treated extracts with Cyclin A, which probably accelerates replication initiation[45]. Plasmid DNA was incubated in High Speed Supernatant for 20 minutes, then either buffer or Cyclin A was added for a further 20 minutes. NucleoPlasmic extract was added to initiate DNA replication, along with [α-^{32}P]dATP to label replication intermediates. Replication products were separated on a native agarose gel, detected by autoradiography (A), and quantified (B). In the presence of vehicle, replication was not complete by 9.5 minutes, but in the presence of Cyclin A,

replication was almost complete by 4.5 minutes (B). Thus, Cyclin A treatment approximately doubles the speed of DNA replication in *Xenopus* egg extracts.

(C–F) To test whether Cyclin A affects the ability of LacR to inhibit termination, we monitored dissolution of plasmids containing a 12x or 16x LacR array in the presence and absence of Cyclin A. p[*lacO*x12], p[*lacO*x16], and the parental control plasmid p[*empty*] were incubated with LacR, and then treated with buffer or Cyclin A before replication was initiated with NPE in the presence of [α-^{32}P]dATP. Samples were withdrawn when dissolution of p[*empty*] plateaued (9.5 minutes in the presence of buffer, 4.5 minutes in the presence of Cyclin A). Given that Cyclin A treatment approximately doubles the speed of replication (see B), samples were withdrawn from these reactions twice as frequently as the buffer-treated samples. To measure dissolution, radiolabelled termination intermediates were cut with XmnI to monitor the conversion of double-Y molecules to linear molecules. Cut molecules were separated on a native agarose gel and detected by autoradiography (C,E). By the time the first sample was withdrawn, dissolution of p[*empty*] was essentially complete, in the absence (9.5 min, D) or presence (4.5 min, F) of Cyclin A. Importantly, dissolution of p[*lacO*x12] and p[*lacO*x16] was prevented in the absence (9.5 min, D) or presence (4.5 min, F) of Cyclin A. Moreover, dissolution occurred approximately twice as fast in the presence of Cyclin A (note the similarity between (D) and (F) even though samples are withdrawn twice as frequently in F.) consistent with replication being approximately twice as fast in the presence of Cyclin A. Therefore, Cyclin A does not affect the ability of a LacR array to block replication forks.

Acknowledgements

References

1. Levine AJ, Kang HS, Billheimer FE. DNA replication in SV40 infected cells IAnalysis of replicating SV40 DNA. J. Mol. Biol. 1970; 50:549–568. [PubMed: 4320050]

2. Fanning E, Zhao K. SV40 DNA replication: from the A gene to a nanomachine. Virology. 2009; 384:352–359. [PubMed: 19101707]

3. Tapper DP, DePamphilis ML. Discontinuous DNA replication: Accumulation of simian virus 40 DNA at specific stages in its replication. J. Mol. Biol. 1978; 120:401–422. [PubMed: 206700]

4. Seidman MM, Salzman NP. Late replicative intermediates are accumulated during simian virus 40 DNA replication in vivo and in vitro. J. Virol. 1979; 30:600–609. [PubMed: 224218]

5. Sundin O, Varshavsky A. Terminal stages of SV40 DNA replication proceed via multiply intertwined catenated dimers. Cell. 1980; 21:103–114. [PubMed: 6250706]

6. Ishimi Y, Sugasawa K, Hanaoka F, Eki T, Hurwitz J. Topoisomerase II plays an essential role as a swivelase in the late stage of SV40 chromosome replication in vitro. J. Biol. Chem. 1992; 267:462–466. [PubMed: 1309747]

7. Hiasa H, Marians KJ. Two distinct modes of strand unlinking during theta-type DNA replication. J. Biol. Chem. 1996; 271:21529–21535. [PubMed: 8702938]

8. Espeli O, Levine C, Hassing H, Marians KJ. Temporal regulation of topoisomerase IV activity in E. coli. Mol. Cell. 2003; 11:189–201. [PubMed: 12535532]

9. Segawa M, Sugano S, Yamaguchi N. Association of simian virus 40 T antigen with replicating nucleoprotein complexes of simian virus 40. J. Virol. 1980; 35:320–330. [PubMed: 6255173]

10. Tack LC, DePamphilis ML. Analysis of simian virus 40 chromosome-T-antigen complexes: T-antigen is preferentially associated with early replicating DNA intermediates. J. Virol. 1983; 48:281–295. [PubMed: 6310148]

11. Chen MC, Birkenmeier E, Salzman NP. Simian virus 40 DNA replication: characterization of gaps in the termination region. J. Virol. 1976; 17:614–621. [PubMed: 176434]

12. Sundin O, Varshavsky A. Arrest of segregation leads to accumulation of highly intertwined catenated dimers: dissection of the final stages of SV40 DNA replication. Cell. 1981; 25:659–669. [PubMed: 6269752]

13. Ivessa AS, Zhou JQ, Zakian VA. The Saccharomyces Pif1p DNA helicase and the highly related Rrm3p have opposite effects on replication fork progression in ribosomal DNA. Cell. 2000; 100:479–489. [PubMed: 10693764]

14. Steinacher R, Osman F, Dalgaard JZ, Lorenz A, Whitby MC. The DNA helicase Pfh1 promotes fork merging at replication termination sites to ensure genome stability. Genes Dev. 2012; 26:594–602. [PubMed: 22426535]

15. Fachinetti D, et al. Replication termination at eukaryotic chromosomes is mediated by Top2 and occurs at genomic loci containing pausing elements. Mol. Cell. 2010; 39:595–605. [PubMed: 20797631]

16. DiNardo S, Voelkel K, Sternglanz R. DNA topoisomerase II mutant of Saccharomyces cerevisiae: topoisomerase II is required for segregation of daughter molecules at the termination of DNA replication. Proc. Natl. Acad. Sci. U. S. A. 1984; 81:2616–2620. [PubMed: 6326134]

17. Baxter J, Diffley JF. Topoisomerase II inactivation prevents the completion of DNA replication in budding yeast. Mol. Cell. 2008; 30:790–802. [PubMed: 18570880]

18. Lucas I, Germe T, Chevrier-Miller M, Hyrien O. Topoisomerase II can unlink replicating DNA by precatenane removal. EMBO J. 2001; 20:6509–6519. [PubMed: 11707421]

19. Gaggioli V, Le Viet B, Germe T, Hyrien O. DNA topoisomerase II controls replication origin cluster licensing and firing time in Xenopus egg extracts. Nucleic Acids Res. 2013

20. Ilves I, Petojevic T, Pesavento JJ, Botchan MR. Activation of the MCM2–7 helicase by association with Cdc45 and GINS proteins. Mol. Cell. 2010; 37:247–258. [PubMed: 20122406]

21. Pacek M, Tutter AV, Kubota Y, Takisawa H, Walter JC. Localization of MCM2–7, Cdc45, and GINS to the site of DNA unwinding during eukaryotic DNA replication. Mol. Cell. 2006; 21:581–587. [PubMed: 16483939]

22. Moyer SE, Lewis PW, Botchan MR. Isolation of the Cdc45/Mcm2–7/GINS (CMG) complex, a candidate for the eukaryotic DNA replication fork helicase. Proc. Natl. Acad. Sci. U. S. A. 2006; 103:10236–10241. [PubMed: 16798881]

23. Kang, YH.; Galal, WC.; Farina, A.; Tappin, I.; Hurwitz, J. Properties of the human Cdc45/Mcm2–7/GINS helicase complex and its action with DNA polymerase epsilon in rolling circle DNA synthesis. Proc. Natl. Acad. Sci. U. S. A. 2012. at <http://www.pnas.org/content/early/2012/03/29/1203734109.long>

24. Maric M, Maculins T, De Piccoli G, Labib K. Cdc48 and a ubiquitin ligase drive disassembly of the CMG helicase at the end of DNA replication. Science (80–.). 2014; 346:1253596–1253596.

25. Priego Moreno S, Bailey R, Campion N, Herron S, Gambus A. Polyubiquitylation drives replisome disassembly at the termination of DNA replication. Science (80–.). 2014; 346:477–481.

26. Hiasa H, Marians KJ. Tus prevents overreplication of oriC plasmid DNA. J. Biol. Chem. 1994; 269:26959–26968. [PubMed: 7929435]

27. Rudolph CJ, Upton AL, Stockum A, Nieduszynski Ca, Lloyd RG. Avoiding chromosome pathology when replication forks collide. Nature. 2013; 500:608–611. [PubMed: 23892781]

28. Hook SS, Lin JJ, Dutta A. Mechanisms to control rereplication and implications for cancer. Curr. Opin. Cell Biol. 2007; 19:663–671. [PubMed: 18053699]

29. Czajkowsky DM, Liu J, Hamlin JL, Shao Z. DNA combing reveals intrinsic temporal disorder in the replication of yeast chromosome VI. J. Mol. Biol. 2008; 375:12–19. [PubMed: 17999930]

30. McGuffee SR, Smith DJ, Whitehouse I. Quantitative, genome-wide analysis of eukaryotic replication initiation and termination. Mol. Cell. 2013; 50:123–135. [PubMed: 23562327]

31. Yardimci H, Loveland AB, Habuchi S, van Oijen AM, Walter JC. Uncoupling of sister replisomes during eukaryotic DNA replication. Mol. Cell. 2010; 40:834–840. [PubMed: 21145490]

32. Loveland AB, Habuchi S, Walter JC, van Oijen AM. A general approach to break the concentration barrier in single-molecule imaging. Nat. Methods. 2012; 9:987–992. [PubMed: 22961247]

33. Santamaría D, et al. Bi-directional replication and random termination. Nucleic Acids Res. 2000; 28:2099–2107. [PubMed: 10773078]

34. Zhang J, et al. DNA interstrand cross-link repair requires replication fork convergence. Nat. Struct. Mol. Biol. In Press

35. Duxin JPP, Dewar JMM, Yardimci H, Walter JCC. Replication-coupled repair of a DNA-protein crosslink. Cell. 2014; 159:346–357. [PubMed: 25303529]

36. Walter J, Sun L, Newport J. Regulated chromosomal DNA replication in the absence of a nucleus. Mol. Cell. 1998; 1:519–529. [PubMed: 9660936]

37. Sofueva S, et al. Ultrafine anaphase bridges, broken DNA and illegitimate recombination induced by a replication fork barrier. Nucleic Acids Res. 2011; 39:6568–6584. [PubMed: 21576223]

38. Charbin A, Bouchoux C, Uhlmann F. Condensin aids sister chromatid decatenation by topoisomerase II. Nucleic Acids Res. 2014; 42:340–348. [PubMed: 24062159]

39. Laskey RA, Mills AD, Morris NR. Assembly of SV40 chromatin in a cell-free system from Xenopus eggs. Cell. 1977; 10:237–243. [PubMed: 189936]

40. Räschle M, et al. Mechanism of replication-coupled DNA interstrand crosslink repair. Cell. 2008; 134:969–980. [PubMed: 18805090]

41. Long DTT, Joukov V, Budzowska M, Walter JCC. BRCA1 Promotes Unloading of the CMG Helicase from a Stalled DNA Replication Fork. Mol. Cell. 2014; 56:174–185. [PubMed: 25219499]

42. Fu YV, et al. Selective bypass of a lagging strand roadblock by the eukaryotic replicative DNA helicase. Cell. 2011; 146:931–941. [PubMed: 21925316]

43. Costa A, et al. The structural basis for MCM2–7 helicase activation by GINS and Cdc45. Nat. Struct. Mol. Biol. 2011; 18:471–477. [PubMed: 21378962]

44. Kaplan DL, Davey MJ, O'Donnell M. Mcm4,6,7 uses a 'pump in ring' mechanism to unwind DNA by steric exclusion and actively translocate along a duplex. J. Biol. Chem. 2003; 278:49171–49182. [PubMed: 13679365]

45. Prokhorova TA, Mowrer K, Gilbert CH, Walter JC. DNA replication of mitotic chromatin in Xenopus egg extracts. Proc. Natl. Acad. Sci. U. S. A. 2003; 100:13241–13246. [PubMed: 14597706]

46. Lebofsky R, Takahashi T, Walter JC. DNA replication in nucleus-free Xenopus egg extracts. Methods Mol. Biol. 2009; 521:229–252. [PubMed: 19563110]

47. Budzowska M, Graham TGW, Sobeck A, Waga S, Walter JC. Regulation of the Rev1-pol ζ complex during bypass of a DNA interstrand cross-link. EMBO J. In Press

48. Magnaghi P, et al. Covalent and allosteric inhibitors of the ATPase VCP/p97 induce cancer cell death. Nat. Chem. Biol. 2013; 9:548–556. [PubMed: 23892893]

49. Walter JC, Newport J. Initiation of eukaryotic DNA replication: origin unwinding and sequential chromatin association of Cdc45, RPA, and DNA polymerase alpha. Mol. Cell. 2000; 5:617–627. [PubMed: 10882098]

Additional Reference

50. Long DT, Räschle M, Joukov V, Walter JC. Mechanism of RAD51-dependent DNA interstrand cross-link repair. Science. 2011; 333:84–87. [PubMed: 21719678]
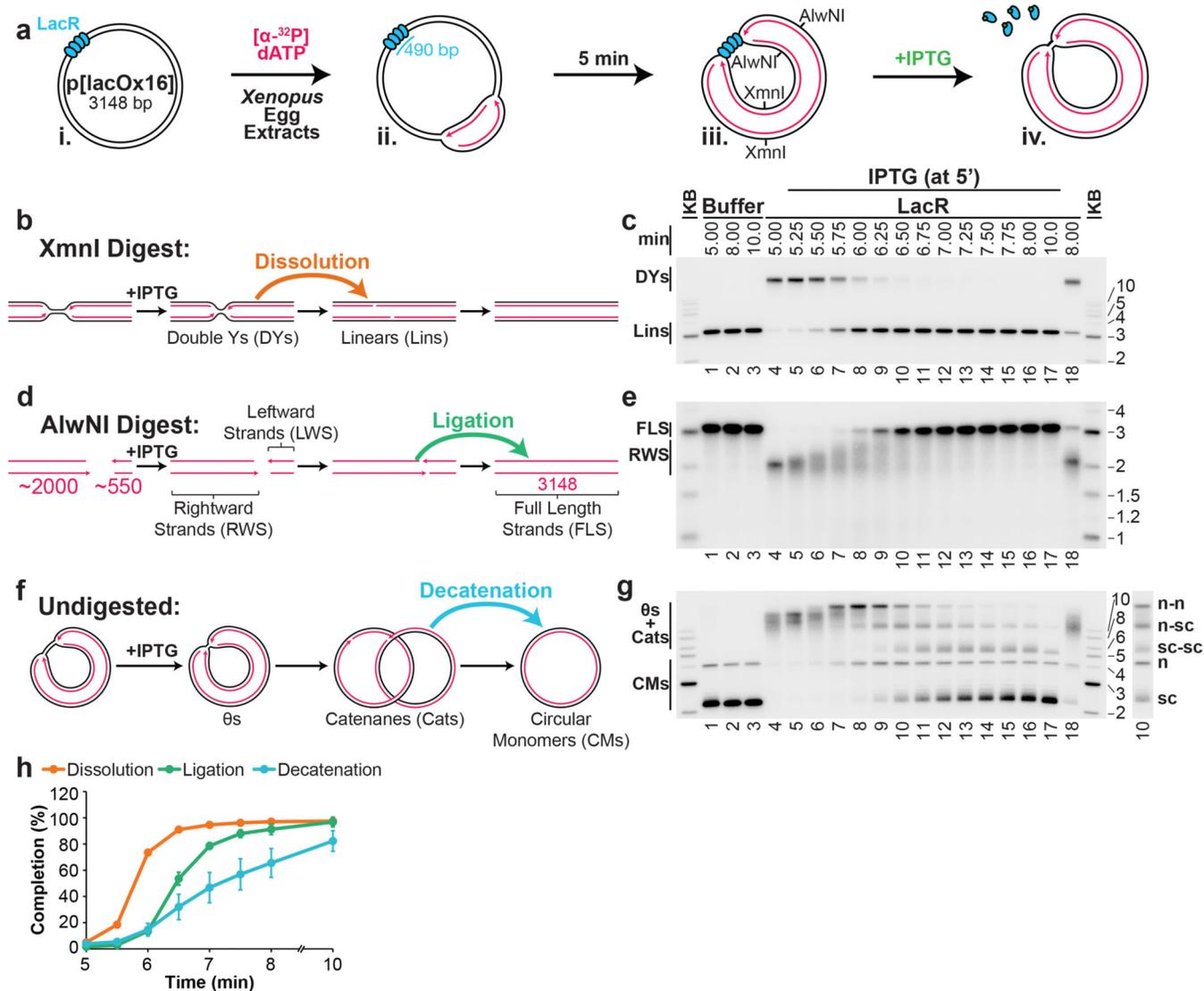
Figure 1. A model system to study replication termination

A. Scheme to induce site-specific termination. Key restriction sites are highlighted.

B. Schematic of the dissolution assay.

C. p[*lacO*x16] was incubated in buffer or LacR, then replicated in the presence of [α-^{32}P]dATP, before termination was induced by the addition of IPTG. To measure *dissolution*, radiolabelled termination intermediates were cut with XmnI, separated on a native agarose gel, and analyzed by autoradiography.

D. Schematic of the ligation assay.

E. To measure *ligation*, replication intermediates were cut with AlwNI and separated on a denaturing agarose gel.

F. Schematic of the decatenation assay

G. To measure *decatenation*, replication intermediates were separated on a native agarose gel. The additional copy of lane 10 highlights catenated termination intermediates.

H. Multiple *dissolution, ligation*, and *decatenation* assays were quantified. Means±standard deviation (s.d.) are plotted (n=4).
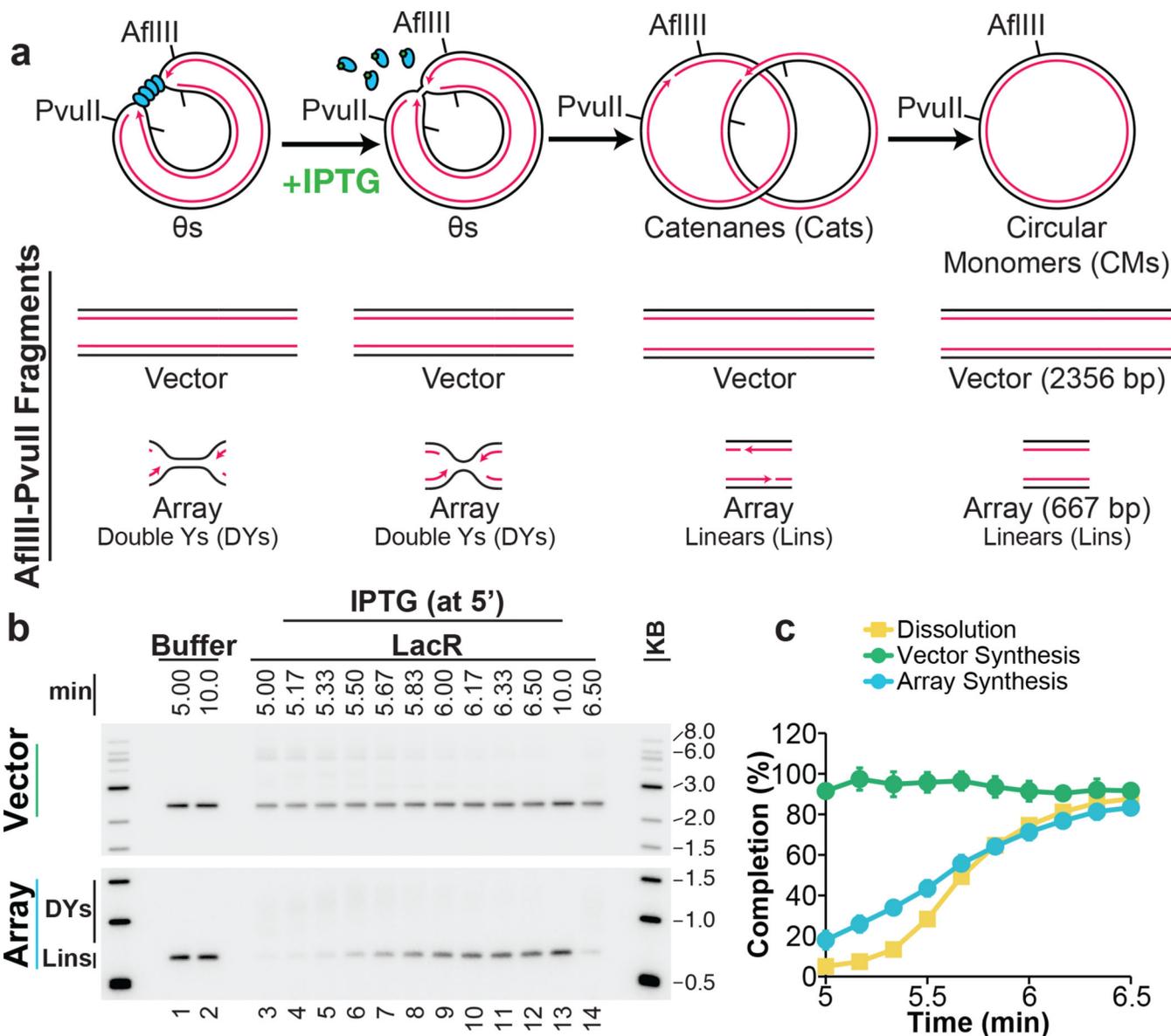
Figure 2. DNA synthesis does not stall during termination

A. Cartoon depicting the assay for *lacO* array synthesis.

B. LacR Block-IPTG release was performed on p[*lacO*x12]. To measure synthesis within the array, termination intermediates were cut with AflIII and PvuII to liberate the array fragment from the vector. Cleaved products were separated by native gel electrophoresis. Different exposures of array and vector fragments are shown (see methods).

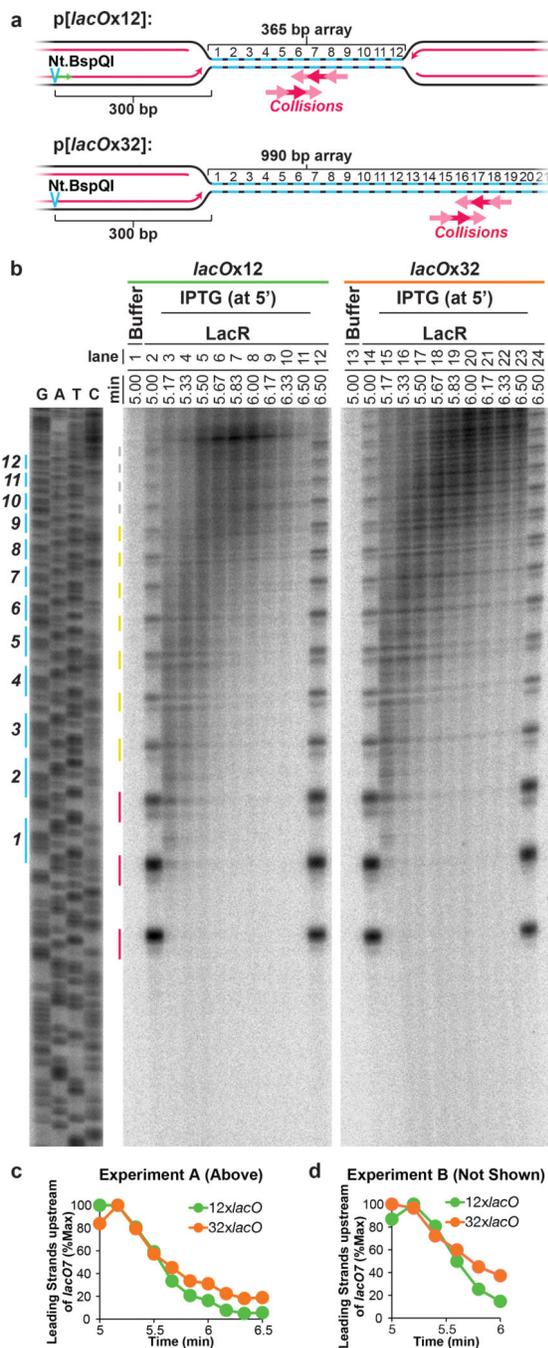C. Array synthesis, vector synthesis, and dissolution were quantified. Means±s.d. are plotted (n=3).

Figure 3. Leading strands pass each other unhindered during termination

A. Schematic of rightward leading strands arrested at 12x and 32x*lacO* arrays, and the predicted point of fork collision upon IPTG addition.

B. LacR block-IPTG release was performed on p[*lacO*x12] and p[*lacO*x32]. Termination intermediates were digested with Nt.BspQI. Nascent strands were separated alongside a sequencing ladder (generated by primer JDO107, green arrow in (A)) on a denaturing polyacrylamide gel and visualized by autoradiography. The *lacO* sites of p[*lacO*x12] are

indicated in blue. Red, yellow, and grey lines indicate stall products that were quantified (Extended Data Fig. 6E).

C. Leading strands whose 3' ends were located before *lacO7* were quantified (see methods) along with dissolution (Extended Data Fig. 6A–D).
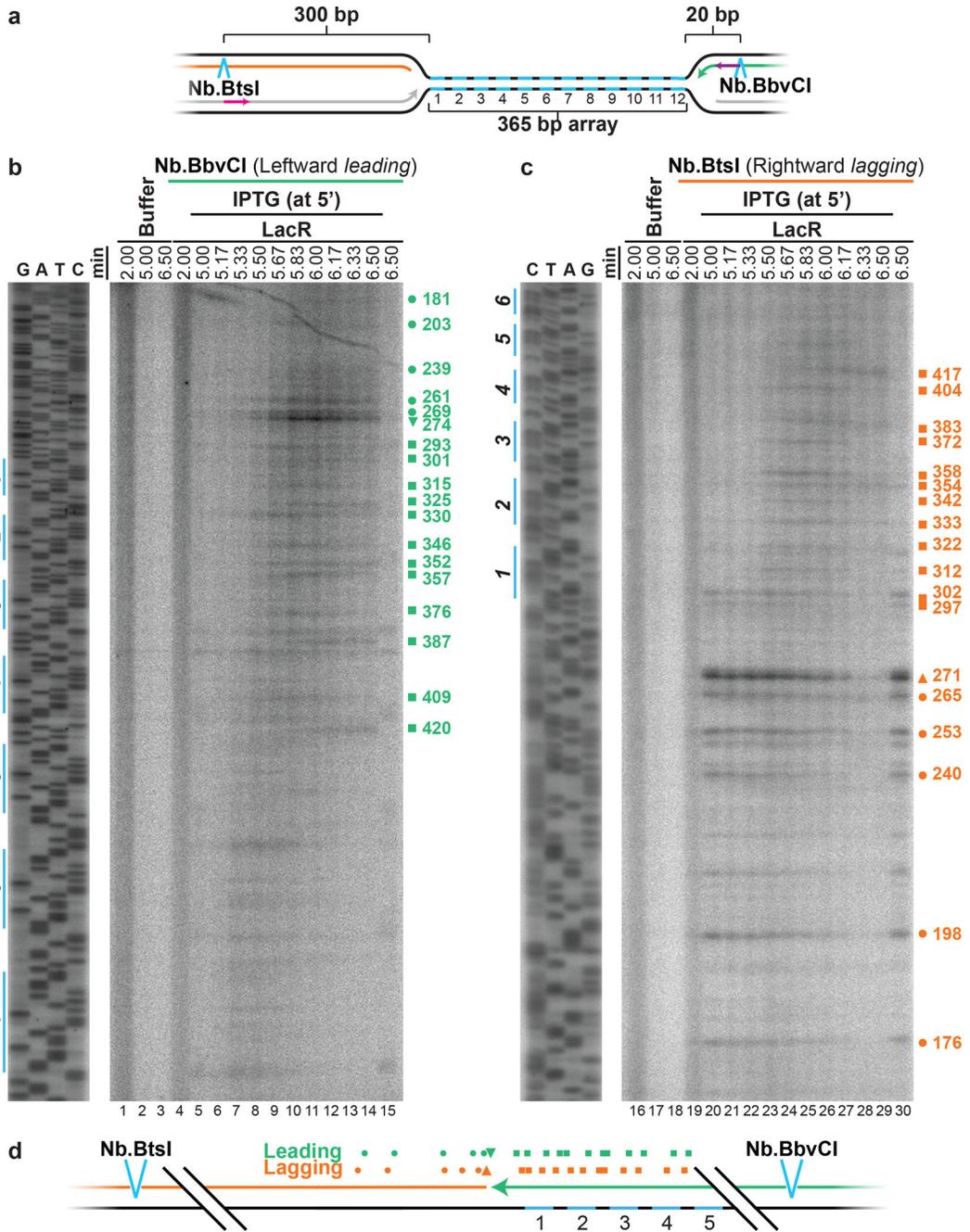
D. Experimental repeat of (C).

Figure 4. Leading strands abut lagging strands of the opposing replisome during termination

A. Cartoon illustrating the leading and lagging strands released by Nb.BtsI and Nb.BbvCI nicking enzymes. Primers JDO111 (purple arrow) and JDO110 (pink arrow) generated the sequencing ladders in (B) and (C), respectively.

B. LacR block-IPTG release was performed on p[*lacO*x12]. Termination intermediates were digested with Nb.BbvCI to liberate *leftward leading* strands, which were separated alongside a sequencing ladder on a denaturing polyacrylamide gel and visualized by autoradiography.

Prominent leading strand products are highlighted (green symbols), and their sizes, measured relative to the Nb.BtsI site, are indicated.

C. Same samples as in (B) were digested with Nb.BtsI to liberate *rightward lagging* strands. The size of prominent lagging strand products (orange symbols), measured relative to the Nb.BtsI site, are indicated.

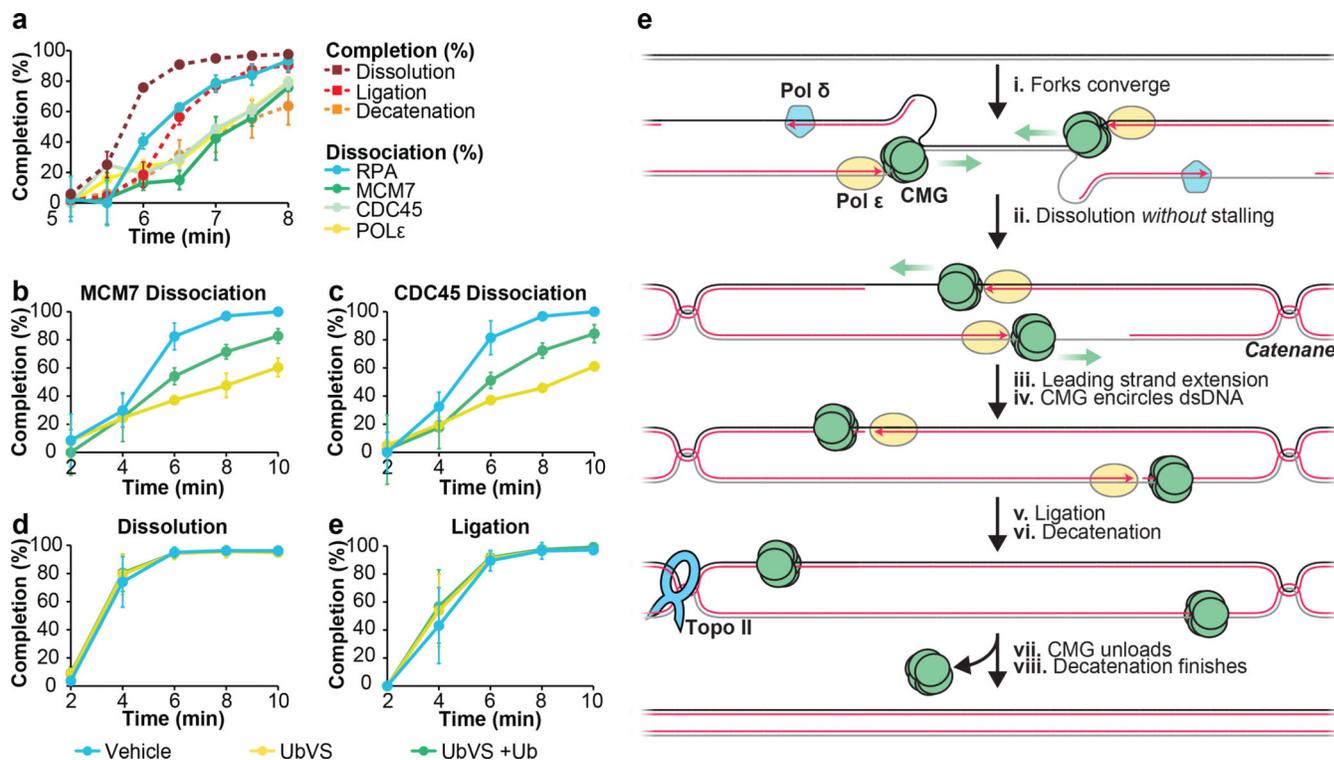D. Schematic of the mapped leading (B) and lagging (C) strands.

Figure 5. CMGs dissociate after dissolution and ligation

A. LacR block-IPTG release was followed by MCM7, CDC45, RPA and, Polε ChIP at the indicated times after IPTG addition. Dissolution, ligation, and decatenation were measured in parallel. means±s.d. are plotted (n=3).

B. p[*empty*] was replicated in extracts treated with Vehicle, Ubiqutin-Vinyl Sulfone (Ub-VS), or Ub-VS and free ubiquitin (UbVS + Ub). Dissociation of MCM7 was measured by ChIP (see methods). mean±s.d. is plotted (n=3).

C. Same as (B), but CDC45 dissociation was measured.

D-E. In parallel to MCM7 and CDC45 dissociation (B, C), dissolution (D) and ligation (E) were measured. mean±s.d. is plotted (n=3). See Extended Data Fig. 8F–I for decatenation measurements and representative gels.

(E) New model of vertebrate replication termination.